Deep Red Luminescence From Platinum(II) Complexes of *N*^*N*⁻^*N*-Amido Ligands With Benzannulated *N*-Heterocyclic Donor Arms

Pavan Mandapati,[a] *Jason D. Braun,*[a] *Issiah B. Lozada,*[a] *J. A. Gareth Williams*[b*] *and David E. Herbert*[a*]

[a] Department of Chemistry and the Manitoba Institute for Materials, University of Manitoba, 144 Dysart Road, Winnipeg, Manitoba, R3T 2N2, Canada

*david.herbert@umanitoba.ca

[b] Department of Chemistry, Durham University, Durham, DH1 3LE, UK

*j.a.g.williams@durham.ac.uk

ABSTRACT

A synthetic methodology for accessing narrow-band, deep-red phosphorescence from mononuclear Pt(II) complexes is presented. These charge-neutral complexes have the general structure (*N*^*N*^*N*)PtCl, in which the Pt(II) centers are supported by benzannulated diarylamido ligand scaffolds bearing substituted quinolinyl and/or phenanthridinyl arms. Emission maxima ranging from 683 to 745 nm are observed with lifetimes spanning from 850 to 4500 ns. In contrast to the corresponding proligands, benzannulation is found to counter-intuitively but markedly blue-shift emission from metal complexes with differing degrees of ligand benzannulation but similar substitution patterns. This effect can be further tuned by incorporation of electron-releasing (Me, *t*Bu) or electron-withdrawing (CF_3) substituents in either the phenanthridine 2-position or quinoline 6-position. Compared with symmetric *bis*(quinoline) and *bis*(phenanthridine) architectures, "mixed" ligands incorporating one quinoline and one phenanthridine unit present a degree of charge transfer between the *N*-heterocyclic arms that is more pronounced in the proligands than in the Pt(II) complexes. The impact of benzannulation and ring-substitution on the structure and photophysical properties of both the proligands and their deep-red emitting Pt(II) complexes is discussed.

INTRODUCTION

Luminescent complexes that emit light in the deep red region of the electromagnetic spectrum are of interest for a variety of applications. For example, white light-emitting diode (LED) devices are commonly constructed by combining high purity red, green and blue emission into a broad spectral output.[1] In addition, deep red and near infrared (NIR) light can penetrate biological tissue to a greater extent than shorter wavelengths and so is more compatible with bioimaging and sensing applications.[2] While fluorescent deep red and NIR emitters have found application in luminescent devices and sensors,[3] phosphorescent complexes present certain distinct advantages.[4] In biosensing/imaging applications, for example, the longer lifetime of phosphorescence can avoid signal complications due to autofluorescence from endogenous fluorophores.[5,6] In LED devices, phosphorescence can enable harvesting of excitons of both singlet and triplet multiplicity.[7]

Efficient, deep red molecular phosphors – emitting from *triplet* states – are not as common as the corresponding fluorescent emitters. Nevertheless, examples built on late transition metal ions are known for elements of Group 7 (Re[8,9]), Group 8 (Ru,[10] Os[11]), Group 9 (Ir[12,13]), Group 10 (Pt[14–17]) and Group 11 (Cu,[18] Au[19]). As a third-row transition element, Pt has a large spin-orbit coupling (SOC) constant that boosts $T_1 \rightarrow S_0$ radiative decay, the formally forbidden phosphorescence process. In addition, the coordination chemistry of Pt is well-established.[20] Taken together, this has led to the design and use of platinum(II) complexes in phosphorescence-based applications including light-emitting diodes,[21–23] bioimaging,[24–26] and chemosensing.[27] The pursuit of deep red Pt(II) emitters is therefore of significant interest. Solution-state emission within this target wavelength region (~700 nm) has been extensively described for Pt(II) complexes with bimolecular excited states (*e.g.*, aggregates or excimers).[28,29] In comparison, complexes that can emit at these wavelengths from monomolecular excited states are very rare, as the extended conjugated systems required typically limit the available supporting ligand platforms to porphyrins or phthalocyanines.[30–33]

In addition to engineering bathochromically shifted emission with narrow profiles, intense absorption of the chromophore in the visible region can also be desirable, particularly in biological media where emissive probes and labels are ideally excited at wavelengths longer than those at which endogenous biological molecules strongly absorb.[34,35] The “brightness” of a

phosphor, defined as the product of the extinction coefficient at the excitation wavelength and the emission quantum yield, is thus a critical parameter.[24] Beyond imaging, in photodynamic therapy (PDT) too, triplet excited states with long enough lifetimes to sensitize singlet oxygen formation are advantageous.[36] Designing molecules which combine strong absorption of visible light with efficient triplet excited-state formation and microsecond lifetimes is also attractive for accessing upconversion via triplet-triplet annihilation (TTA-UC).[37]

We recently reported a series of Pt(II) complexes that to date present some of the most red-shifted phosphorescence for non-porphyrinic Pt(II) complexes emitting from monomolecular excited states.[38] These complexes are based on anionic, tridentate pincer-like ligands, with the form (*N*^*N*^*N*)PtCl. In this work, we extend our synthetic strategy and demonstrate how ligand substitution can be used to further tune the emission properties of a rare class of mononuclear Pt(II) deep red emitters.

RESULTS AND DISCUSSION

Ligand Preparation and Scope

To build our library of ligands, functionalized amino/bromoquinolines and phenanthridines bearing either electron-withdrawing (EWG: CF_3), electron-donating (EDG: CH_3, *t*Bu) groups, or no substituent (H) on the heterocycle were synthesized (Scheme 1). Phenanthridine precursors were prepared using tandem Pd-catalyzed cross-coupling/condensation reactions of 2-formylphenylboronic acid and appropriately substituted anilines, following a protocol we previously established.[39] Quinoline precursors were prepared using Skraup reaction conditions.[40] For the tricyclic systems, formation of the phenanthridine core was confirmed in each case by the appearance of a diagnostic proton resonance between 9.35 and 9.50 ppm, attributed to the N=C*H* in the 6-position of the heterocycle (Table S1).[41] Once in hand, the amino- and bromo-substituted heterocycles were subjected to Buchwald-Hartwig amination conditions, similar to those reported for the synthesis of the *bis*(quinolinyl)amine $\mathbf{L1^{H,H}}$.[42] In general, proligand synthesis proceeded efficiently and twelve *bis*(*N*-heterocyclic)amines with a variety of substitution patterns (grouped into $\mathbf{L1^{R,R}}$, $\mathbf{L2^{R,R}}$, $\mathbf{L3^{R,R}}$) were isolated in good yields (70-90%) as orange-red ($\mathbf{L2^{Me,tBu}}$) or yellow-green solids following chromatography. The $\mathbf{L1^{R,R}}$ and $\mathbf{L3^{R,R}}$ proligands are

bis(quinolyl)amines and *bis*(phenanthridinyl)amines respectively; superscripts are used to denote the substituents *meta* to the amine N–H. These proligands are symmetric around the N–H, apart from $\mathbf{L3}^{\mathbf{CF3,}t\mathbf{Bu}}$ which comprises two differently substituted phenanthridines. Within the $\mathbf{L2}^{\mathbf{R,R}}$ group, in contrast, each proligand contains one phenanthridine and one quinoline donor.

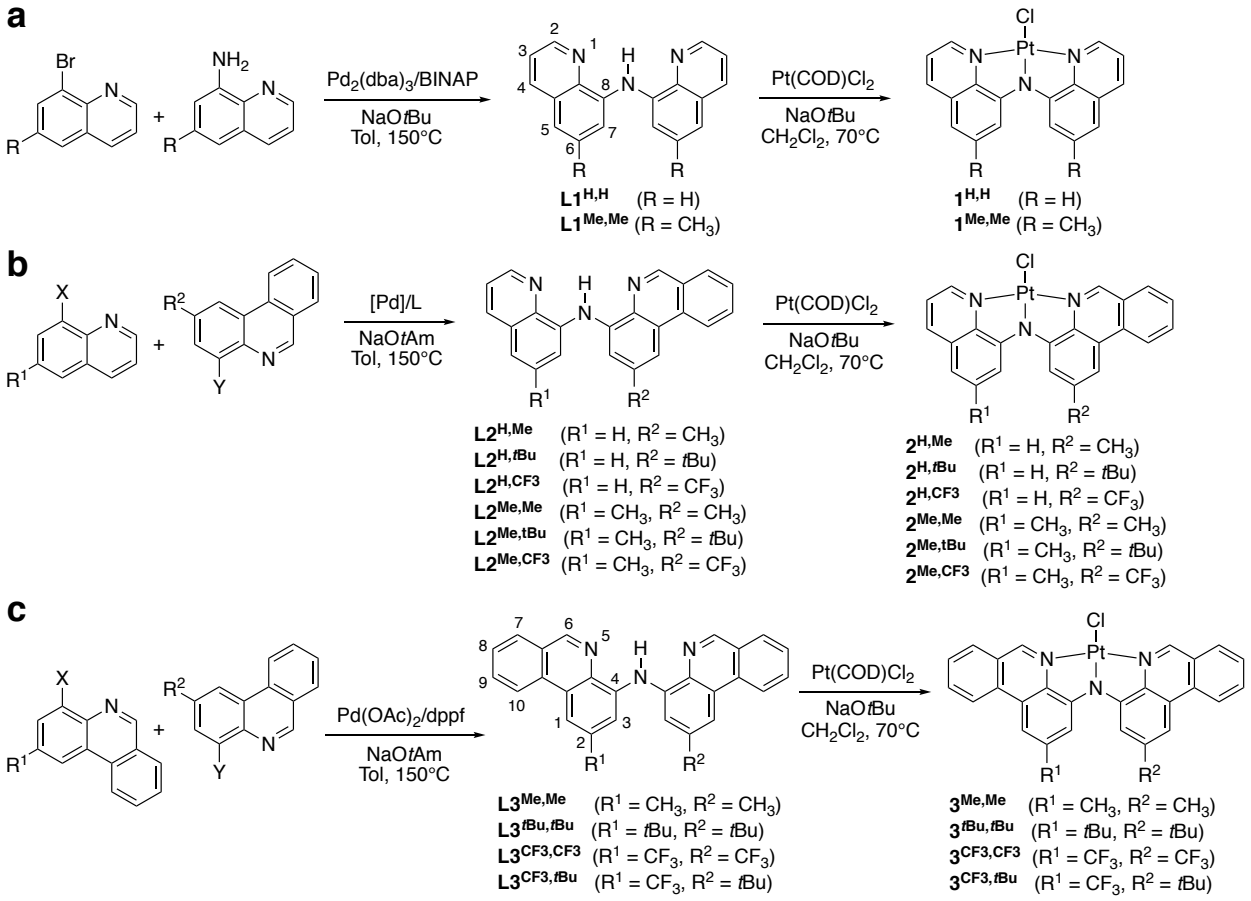

Scheme 1. Synthetic routes to proligands (a) $\mathbf{L1}^{\mathbf{H,H}}$ [42] and $\mathbf{L1}^{\mathbf{Me,Me}}$ [38]; (b) $\mathbf{L2}^{\mathbf{H,Me}}$ [43], $\mathbf{L2}^{\mathbf{H},t\mathbf{Bu}}$ [44], $\mathbf{L2}^{\mathbf{H,CF3}}$ [44] (R^1 = H, X = NH_2; R^2 = CF_3, Y = Br; [Pd] = $Pd_2(dba)_3$, L = *rac*-BINAP); $\mathbf{L2}^{\mathbf{Me,Me}}$ [38]; $\mathbf{L2}^{\mathbf{Me},t\mathbf{Bu}}$ (R^1 = CH_3, X = Br; R^2 = *t*Bu, Y = NH_2; [Pd] = $Pd_2(dba)_3$, L = *rac*-BINAP), $\mathbf{L2}^{\mathbf{Me,CF3}}$ (R^1 = CH_3, X = NH_2; R^2 = CF_3, Y = Br; [Pd] = $Pd(OAc)_2$, L = dppf); (c) $\mathbf{L3}^{\mathbf{Me,Me}}$ [43], $\mathbf{L3}^{t\mathbf{Bu},t\mathbf{Bu}}$, $\mathbf{L3}^{\mathbf{CF3,CF3}}$, $\mathbf{L3}^{t\mathbf{Bu,CF3}}$. The preparation and structures of their corresponding (*N*^*N*⁻^*N*)PtCl complexes $\mathbf{1}^{\mathbf{R,R}}/\mathbf{2}^{\mathbf{R,R}}/\mathbf{3}^{\mathbf{R,R}}$ are also shown. The IUPAC numbering system for quinolines and phenanthridines is illustrated for $\mathbf{L1}^{\mathbf{R,R}}$ and $\mathbf{L3}^{\mathbf{R,R}}$.

The proligands were characterized by ^{1}H, ^{13}C and ^{19}F (for the CF_3 derivatives) NMR spectroscopy in solution (see Table S1 for selected ^{1}H NMR resonances). The crystal structure of a representative proligand (**L3**^{CF3,CF3}) was obtained to verify the solution-state structure assigned by NMR (Figure 1). Appendage of two, 2-substituted phenanthridinyl rings about the central N–H unit can be clearly seen in the solid state. The importance of the 'imine-bridged biphenyl' resonance contributor to the ground state of phenanthridine derivatives is evident in the comparably short C1-N1 [1.301(4) Å] and C15-N3 distances [1.301(3) Å]. Unlike related diarylamine proligands, **L3**^{CF3,CF3} is essentially flat in the solid state, likely a result of packing effects; π-stacking is evidenced by contacts of < 3.4 Å between neighboring phenanthridine units which are staggered head-to-tail relative to one another (Figure S1).

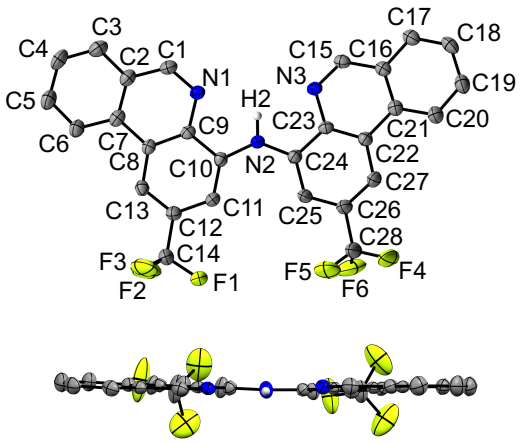

Figure 1. Solid-state structure of **L3**^{CF3,CF3} with thermal ellipsoids at 50% probability and hydrogen atoms omitted for clarity. Selected bond distances (Å) and angles (°): N(1)–C(1) 1.301(4), N(2)–C(10) 1.380(3), N(2)–C(24) 1.375(3), N(3)–C(15) 1.301(3); C(10)-N(2)-C(24) 132.9(2).

With the proligands in hand, a full library of Pt(II) complexes (series **1**^{R,R}, **2**^{R,R}, **3**^{R,R} from **L1**^{R,R}, **L2**^{R,R}, **L3**^{R,R}) was prepared by reluxing dichloromethane solutions of proligand and $Pt(COD)Cl_2$ (COD = 1,5-cyclooctadiene) in the presence of a base (sodium *tert*-butoxide). Over the course of the reaction, the complexes were observed to precipitate as dark red solids. They are all poorly soluble in common organic solvents, and solubility was further diminished by benzannulation despite the introduction of substituents such as *t*Bu or CF_3 onto the *N*-heterocyclic arms of **2**^{R,R} and **3**^{R,R}. Nonetheless, solution-state ^{1}H NMR spectroscopy verified

ligand binding, as the 6-positioned [C*H*] resonance of the phenanthridinyl arms of $\mathbf{L2^{R,R}}$ and $\mathbf{L3^{R,R}}$ shifted in a diagnostic fashion upon coordination (Table S1). When resolved, $^{3}J_{PtH}$ coupling constants of 33-39 Hz could be observed between the coordinated Pt and the hydrogen nucleus *ortho* to the donor nitrogen of the heterocyclic ligand. In this way, we were able to establish the structures of the library of compounds in solution. Compound purity in the solid-state was confirmed using combustion analysis.

The crystal structures of $\mathbf{2^{Me,tBu}}$ and $\mathbf{3^{tBu,tBu}}$ are shown in Figure 2. As with previously reported structures of $\mathbf{1^{H,H}}$,[42] $\mathbf{1^{Me,Me}}$,[38] $\mathbf{2^{H,Me}}$ and $\mathbf{3^{Me,Me}}$,[43] the coordinated ligands bind in a meridional fashion to each Pt center and form planar structures. The structure of $\mathbf{2^{Me,tBu}}$ does not contain any solvent molecules embedded in the crystal lattice, while that of $\mathbf{3^{tBu,tBu}}$ reveals a co-crystallized equivalent of CH_2Cl_2. Close intermolecular π-π interactions (3.3-3.5 Å) can be discerned in the structure of $\mathbf{2^{Me,tBu}}$ (Figure S2); in that of $\mathbf{3^{tBu,tBu}}$, they are replaced by non-covalent interactions with co-crystallized CH_2Cl_2 solvent (Figure S3). The trend of decreasing solubility within the series $\mathbf{1^{R,R}} > \mathbf{2^{R,R}} > \mathbf{3^{R,R}}$ likely arises from the presence of π-π interactions similar to those seen in structure of $\mathbf{2^{Me,tBu}}$, which are plausibly enhanced by benzannulation. Thus, crystals of $\mathbf{3^{tBu,tBu}}$ suitable for diffraction could only be grown through disruption of these interactions by inclusion of solvent in the lattice.

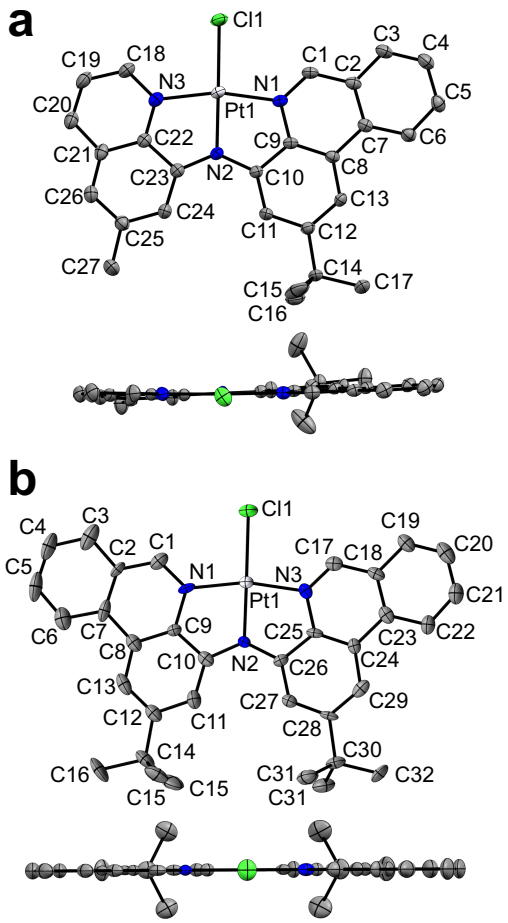

Figure 2. Solid-state structures of (a) $\mathbf{2}^{\mathbf{Me,}t\mathbf{Bu}}$ and (b) $\mathbf{3}^{t\mathbf{Bu,}t\mathbf{Bu}}$ with thermal ellipsoids at 50% probability and hydrogen atoms omitted for clarity. For each structure, views perpendicular to the metal square plane (top) and along the Cl–Pt–N(2) axis (bottom) are shown. Selected bond distances (Å) and angles (°) for $\mathbf{2}^{\mathbf{Me,}t\mathbf{Bu}}$: Cl(1)–Pt(1) 2.3307(6), N(1)–Pt(1) 1.9918(18), N(2)–Pt(1) 1.9736(18), N(3)–Pt(1) 1.9950(19), N(1)–C(1) 1.314(3), N(3)–C(18) 1.336(3); N(1)-Pt(1)-N(3)165.62(7), N(2)-Pt(1)-Cl(1) 178.55(5), N(1)-Pt(1)-Cl(1) 97.37(5), N(3)-Pt(1)-Cl(1) 97.00(6), N(2)-Pt(1)-N(1) 83.06(7), N(2)-Pt(1)-N(3) 82.60(7), C(10)-N(2)-C(23) 131.27(18). $\mathbf{3}^{t\mathbf{Bu,}t\mathbf{Bu}}$: Cl(1)–Pt(1) 2.337(2), N(1)–Pt(1) 1.996(8), N(2)–Pt(1) 1.950(7), N(3)–Pt(1) 1.998(8), N(1)–C(1) 1.287(13), N(3)–C(17) 1.292(13); N(1)-Pt(1)-N(3) 165.9(3), N(2)-Pt(1)-Cl(1) 179.4(3), N(1)-Pt(1)-Cl(1) 96.0(3), N(3)-Pt(1)-Cl(1) 98.1(3), N(2)-Pt(1)-N(1) 83.4(4), N(2)-Pt(1)-N(3) 82.5(3), C(10)-N(2)-C(26) 130.1(8).

Photophysical Properties

Extension of a conjugated ligand's π-system through benzannulation and introducing donor or acceptor substituents represent two common strategies for red-shifting emission from transition metal coordination complexes without introducing significant changes to the parent structure. Thompson and coworkers have shown that the structure-property relationship between benzannulation and absorption/emission, however, is more nuanced than is often supposed.[45] In that study, they demonstrated that the effect of benzannulation must be evaluated in light of the site of benzannulation and the localization of the frontier orbitals for systems in which the lowest energy spin-allowed absorption and spin-forbidden emitting state involve HOMO-LUMO transitions. This new paradigm has been verified for 1,3-*bis*(2-pyridylimino)isoindoline-supported platinum chlorides, various organic emitters,[45] and phosphorescent cyclometallated Ir(III) complexes.[46] For platinum chloride complexes supported by *bis*(8-quinolinyl)amido ligands (*e.g.*, $\mathbf{1}^{\mathbf{Me,Me}}$), *bis*(phenanthridinyl)amido ligands ($\mathbf{3}^{\mathbf{Me,Me}}$) and "mixed" analogues ($\mathbf{2}^{\mathbf{Me,Me}}$) that incorporate one quinoline and one phenanthridine, however, we have discovered that this model does not fully hold.[38] In these compounds, absorption and emission are not affected in the same way by benzannulation; all three complexes show isoenergetic absorption maxima, but emission from the complex with the most extended ligand π-system $\mathbf{3}^{\mathbf{Me,Me}}$ is blue-shifted by nearly 40 nm. Similarly exceptional behaviour was observed for phenanthridinyl and quinolinyl derivatives of $(P\text{^}N)_2CuX_2$ dimers.[47] In that case, emission was shifted to higher energy for complexes of phenanthridinyl ligands despite a red-shift in absorption. The library of proligands presented here enables both further insight into the impact of π-extension and also how substitution patterns of benzannulated ligands affect absorption and emission.

Proligands L1–L3

The photophysical properties of the proligands are considered first, followed by those of the corresponding Pt(II) complexes. Table 1 compiles room temperature absorption and emission data in dichloromethane solution for all twelve proligands, with a selection of representative spectra shown in Figure 3 (absorption) and Figure 4 (emission). In our initial report,[38] we considered only the dimethylated compounds $\mathbf{L1}^{\mathbf{Me,Me}}$, $\mathbf{L2}^{\mathbf{Me,Me}}$ and $\mathbf{L3}^{\mathbf{Me,Me}}$ in order to isolate the effect of benzannulation by keeping ring substitution patterns consistent. All three proligands were found to show a strong, lowest energy absorption band centered around 400 nm. Although

this band appears to be shifted slightly to higher energy in the phenanthridine-containing systems $\mathbf{L2^{R,R}}$, $\mathbf{L3^{R,R}}$ relative to the *bis*(quinoline) congener $\mathbf{L1^{Me,Me}}$ in terms of the λ_{max} value (Table 1, Figure 3), the former tail further into the visible and absorb more intensely at wavelengths greater than 415 nm. The first spin-allowed transition may thus be lower in energy for the phenanthridine-containing molecules which present more extended π systems, as would be anticipated based on the first singlet excited state energies of the constituent heterocycles (E_S of quinoline and phenanthridine are 31850 and 28590 cm^{-1} respectively[48]).

With the new proligand derivatives in hand, the effects of ring substitution can now be evaluated too. Considering the *bis*(phenanthridine) systems ($\mathbf{L3^{R,R}}$, Figure 3a), it can be seen that the replacement of the methyl substituents at the 2-position by electron-withdrawing trifluoromethyl groups leads to a blue-shift in the lowest energy absorption band, while changing to *t*Bu substituents has little effect on λ_{max} though the band is broadened slightly (Note: these shifts are best examined by referring to the spectra, rather than the λ_{max} values which do not necessarily capture the full picture; see Figure S4). The band of the mixed-substituent $\mathbf{L3^{CF3,tBu}}$ is also rather broad, but has a shorter λ_{max} similar to $\mathbf{L3^{CF3,CF3}}$. These observations can be rationalized by considering the localization of the frontier orbitals. We previously demonstrated using density functional theory (DFT) and time-dependent DFT (TDDFT) calculations that the lowest energy transitions of $\mathbf{L1^{Me,Me}}$-$\mathbf{L3^{Me,Me}}$ are HOMO→LUMO in nature.[38] The HOMOs of these systems are comprised of the amine lone pair (:NH; ~20%) and the C_6 ring of the heterocycle arms directly bonded to the amine unit (~34% from each arm). The LUMOs, in comparison, are made up of out-of-phase (π*) contributions from the π systems of the *N*-heterocycles, specifically the C_5N rings (~24% per *N*-heterocycle) and the C=N subunit in particular.[38] Ring substitution at the 2-position of the phenanthridinyl rings in $\mathbf{L3^{R,R}}$ most directly impacts the HOMO, being directly attached to the C_6 ring comprising ~70% of this frontier orbital. Substitution with a strongly electron-withdrawing CF_3 group has a stabilizing effect on the HOMO, widening the HOMO-LUMO gap, leading to the observed blue shift. CF_3 has a greater (electron-withdrawing) effect compared with the (electron-releasing) impact of *t*Bu, as evidenced by the absolute values of their respective Hammett parameters (CF_3: $\sigma_{meta} = 0.43$; *t*Bu: $\sigma_{meta} = -0.10$)[49,50] and thus the impact of substitution on the HOMO is more pronounced in $\mathbf{L3^{CF3,CF3}}$.

The "mixed" quinoline-phenanthridine systems $\mathbf{L2}^{\mathbf{R,R}}$ show a similar trend on variation of the phenanthridine substituent (Figure 3b), with the lowest energy absorption in $\mathbf{L2}^{\mathbf{Me,CF3}}$ blue-shifted relative to the dimethyl and *t*Bu analogues. A strong band at around 310 nm – which is a feature of the *bis*(phenanthridine) $\mathbf{L3}^{\mathbf{R,R}}$ series but not of the *bis*(quinolines) $\mathbf{L1}^{\mathbf{R,R}}$ – also appears in the mixed $\mathbf{L2}^{\mathbf{R,R}}$ compounds but is proportionately weaker than in $\mathbf{L3}^{\mathbf{R,R}}$, consistent with the presence of one of each type of heterocycle.[38] The $\mathbf{L2}^{\mathbf{H,R}}$ compounds (with no substituent on the quinoline) show exactly the same trend (Figure S5), and there is no significant difference in their absorption spectra compared to their respective methylated quinoline analogs $\mathbf{L2}^{\mathbf{Me,R}}$.

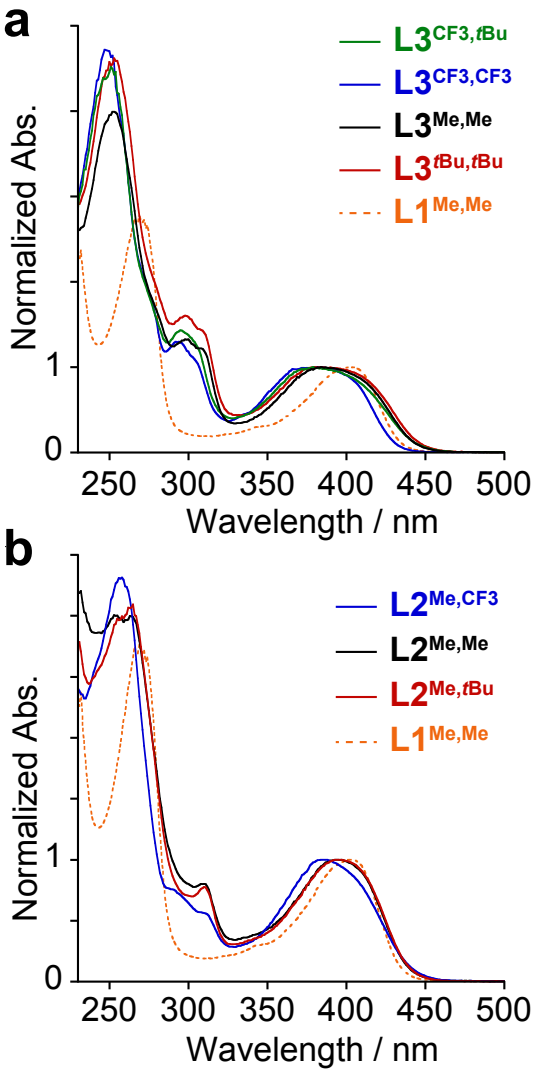

Figure 3. UV-visible absorption spectra in CH_2Cl_2 solution at 295 K of (a) *bis*(phenanthridine) proligands $\mathbf{L3}^{\mathbf{R,R}}$; (b) three of the mixed quinoline-phenanthridine $\mathbf{L2}^{\mathbf{Me,R}}$ ($\mathbf{L2}^{\mathbf{H,R}}$ are shown in Figure S5). In both panels, the absorption spectrum of the *bis*(quinoline) proligand $\mathbf{L1}^{\mathbf{Me,Me}}$ is provided for comparison.

Table 1. Absorption and emission data of proligands in CH_2Cl_2 at 295 K and in EPA (diethyl ether/isopentane/ethanol, 2:2:1 v/v) glass at 77 K.

Proligand	Absorption λ_{max} / nm (ε / M^{-1} cm^{-1})	Emission λ_{max} / nm	Φ_{lum} × 10^2	Emission 77 K	
				λ_{max} / nm	τ / ns
L1^{H,H}	270 (23000), 342 (sh), 403 (9520)	475	0.35	429, 449	3.7
L1^{Me,Me}	269 (28400), 344 (3200), 403 (9800)	474	0.55	431, 451	3.5
L2^{H,Me}	254 (23900), 265 (23800), 310 (6410), 395 (8910)	497	0.16	445, 468	5.0
L2^{H,tBu}	254 (27700), 264 (27900), 309 (7640), 397 (9320)	493	0.23	437, 456	3.6
L2^{H,CF3}	255 (26800), 290 (6060), 309 (4890), 386 (9050)	509	0.10	444, 467	2.2
L2^{Me,Me}	254 (26000), 264 (27100), 310 (7400), 395 (9000)	503	0.25	441, 461	3.8
L2^{Me,tBu}	255 (28200), 265 (29300), 311 (7300), 394 (9480)	505	0.19	437, 455	3.4
L2^{Me,CF3}	257 (30200), 291 (6860), 310 (5120), 386 (9140)	518	0.12	445, 467	2.0
L3^{Me,Me}	253 (65200), 299 (22000), 308 (sh), 388 (15900)	485	0.20	447, 471	3.2
L3^{tBu,tBu}	253 (76100), 299 (26400), 309 (sh), 383 (16500)	498	0.47	443, 467, 508, 551	3.9
L3^{CF3,CF3}	247 (76000), 294 (20900), 304 (sh), 382 (16100)	476	0.098	423, 447	2.0
L3^{CF3,tBu}	254 (75400), 296 (21600), 380 (16900)	518	0.21	445, 469	3.8

At room temperature, the twelve proligands all emit weakly in solution, with unstructured and broad fluorescence peaking at ~ 474–518 nm, quantum yields below 1% and lifetimes of less than 1 ns (Figure 4 and Table 1). We noted in our initial report[38] how emission from the *bis*(quinoline) **L1^{Me,Me}** occurs at higher energy than either of the phenanthridine-containing molecules. This trend is likewise observed in all of the new proligands reported here, consistent

with the previously mentioned trend in the first singlet excited state energy (E_s) of the parent heterocycles.

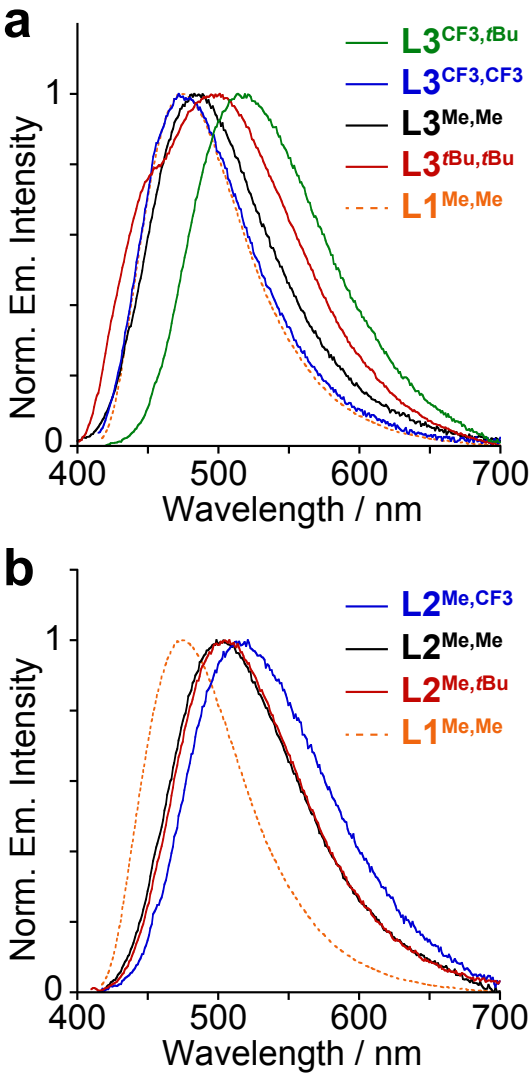

Figure 4. Photoluminescence spectra in CH_2Cl_2 solution at 295 K of (a) *bis*(phenanthridine) proligands $\mathbf{L3^{R,R}}$; (b) three of the mixed quinoline-phenanthridine $\mathbf{L2^{Me,R}}$ ($\mathbf{L2^{H,R}}$ are shown in Figure S6). In both panels, the emission spectrum of the *bis*(quinoline) proligand $\mathbf{L1^{Me,Me}}$ is provided for comparison.

Amongst the three symmetrically substituted *bis*(phenanthridine) ligands, $\mathbf{L3^{CF3,CF3}}$ emits at highest energy and $\mathbf{L3^{tBu,tBu}}$ the lowest (Figure 4a). Interestingly, however, the asymmetric derivative $\mathbf{L3^{CF3,tBu}}$ emits at unequivocally lower energy than either of them, indicative of an element of charge-transfer character between the differently substituted phenanthridines. A

similar observation is made for the $\mathbf{L2}^{\mathbf{R,R}}$ series: $\mathbf{L2}^{\mathbf{Me,CF3}}$ emits at a lower energy than $\mathbf{L2}^{\mathbf{Me,Me}}$ or $\mathbf{L2}^{\mathbf{Me,}t\mathbf{Bu}}$ (Figure 4b), while $\mathbf{L2}^{\mathbf{H,CF3}}$ emits at a lower energy compared to $\mathbf{L2}^{\mathbf{H,Me}}$ and $\mathbf{L2}^{\mathbf{H,}t\mathbf{Bu}}$ (Figure S6). Across the entire library, the mixed quinoline-phenanthridine compounds $\mathbf{L2}^{\mathbf{R,R}}$ are all red-shifted compared to their correspondingly substituted *bis*(phenanthridine) analogues $\mathbf{L3}^{\mathbf{R,R}}$, consistent with the quinoline and phenanthridine units acting as donor and acceptor respectively in a charge-transfer process. At 77 K (Table 1, Figure S7), this effect is largely lost which may be understood in terms of a destabilization of the charge-transfer contribution under these conditions. Underscoring this point, the three compounds incorporating a methyl substituent in the 6-position of the quinoline arm ($\mathbf{L2}^{\mathbf{Me,R}}$) all show a small but significant red-shift relative to those with no substituent on the quinoline ($\mathbf{L2}^{\mathbf{H,R}}$) at room temperature (Figure S8). This is consistent with the methylated quinoline being a slightly more electron-rich donor in the proposed charge-transfer process.

Platinum complexes

Photophysical data for all twelve of the platinum complexes are reported in Table 2, with selected UV-visible absorption spectra shown in Figure 5 (additional absorption and emission spectra are shown in Figures S9 and S10). The Pt complexes are all dark red in color. Accordingly, a broad and intense absorption band can be observed in each case, with a maximum at ~500 nm. Deprotonation of the amine N–H and chelation to a Lewis acidic Pt(II) center thus increases the energy of the highest occupied orbitals and concomitantly stabilizes the heterocycle-based π* orbitals, displacing the lowest energy absorption band by ~5000 cm^{-1} compared with the proligands. The major difference between the phenanthridine-containing complexes ($\mathbf{2}^{\mathbf{R,R}}$ and $\mathbf{3}^{\mathbf{R,R}}$) and the *bis*(quinoline) analogs ($\mathbf{1}^{\mathbf{R,R}}$) is the higher absorption of the former in the 300–350 nm region, as observed for the proligands. The identity of the substituents in the 2-position of the phenanthridine (or the 6-position of the quinoline)[41] is seen to have minimal effect on the lowest-energy absorption band. As demonstrated for the methyl substituted analogs $\mathbf{1}^{\mathbf{Me,Me}}$-$\mathbf{3}^{\mathbf{Me,Me}}$, the main contributor to the lowest energy absorption is the HOMO→LUMO+1 transition.[38] Population analysis of both these orbitals revealed only small contributions of the carbon at the site of substitution. For example, there is no orbital density present at the carbons directly bonded to the methyl groups, nor at the methyl groups themselves,

in the HOMOs of $\mathbf{1}^{\mathbf{Me,Me}}$-$\mathbf{3}^{\mathbf{Me,Me}}$. Thus, only the *bis*-$CF_3$-substituted complex, bearing strongly electron-withdrawing substituents, shows some differences in relative intensities of UV and visible bands compared to the others (Figure 5a). Nevertheless, only a small shift to lower energy is observed for the lowest energy absorption in $\mathbf{3}^{\mathbf{CF3,CF3}}$ compared with $\mathbf{3}^{\mathbf{Me,Me}}$.

Table 2. Absorption and emission data of Pt(II) complexes[a]

	Absorption λ_{max}/nm	Emission λ_{max}/nm[b]	$\Phi_{lum} \times 10^2$ [b,c]	τ / ns [d]	$k_r / 10^3$ s^{-1} [e]	$\Sigma k_{nr} / 10^5$ s^{-1} [e]	$k_Q^{O2} / 10^9$ $M^{-1}s^{-1}$ [f]	Emission 77 K[g] λ_{max}/nm [h]	Emission 77 K[g] τ / ns
$\mathbf{1}^{\mathbf{H,H}}$	239, 300, 342, 357, 381, **504**	740	0.10	1200 [170]	0.83	8.3	2.3	692, 760	3300
$\mathbf{1}^{\mathbf{Me,Me}}$	240, 301, 340, 356, 381, **501**	738	0.081	1800 [230]	0.49	5.6	1.7	696, 763	2200
$\mathbf{2}^{\mathbf{H,Me}}$	244, 258, 284, 315, 338, 353, 404, **504**	745	0.11	1100 [180]	1.0	9.1	2.1	692,753	5200
$\mathbf{2}^{\mathbf{H,}t\mathbf{Bu}}$	245, 260, 280sh, 317, 338, 356, 403, **508**	737	0.22	1800 [190]	1.2	5.5	2.1	682,741	2900
$\mathbf{2}^{\mathbf{H,CF3}}$	235, 261, 283, 325, 356, 412, **500**	712	0.31	2000 [250]	1.6	5.0	1.6	680, 726	6500
$\mathbf{2}^{\mathbf{Me,Me}}$	246, 284, 315, 338, 354, 405, **502**	740	0.13	1000 [180]	1.3	10	2.1	692, 756	3000
$\mathbf{2}^{\mathbf{Me,}t\mathbf{Bu}}$	243, 285, 316, 338, 355, 405, **505**	743	0.092	850 [220]	1.1	12	1.5	690, 753	5600
$\mathbf{2}^{\mathbf{Me,CF3}}$	236, 261, 282, 324, 356, 415, **497**, 570sh	710	0.30	2000 [210]	1.5	5.0	1.9	711, 774	2600
$\mathbf{3}^{\mathbf{Me,Me}}$	265, 321, 338, 355, 405, **503**	703	0.18	2500 [190]	0.72	4.0	2.2	663, 727	18300
$\mathbf{3}^{t\mathbf{Bu},t\mathbf{Bu}}$	266, 324, 338, 356, 406, **509**	713	0.47	2000 [190]	2.4	5.0	2.2	664, 728	2600
$\mathbf{3}^{\mathbf{CF3,CF3}}$	241, 263, 330, 348, 369, 404sh, **506**, 539sh	683	0.10	4500 [240]	0.22	2.2	1.8	675	1800
$\mathbf{3}^{\mathbf{CF3,}t\mathbf{Bu}}$	265, 325, 337, 356, 399, **502**, 570sh	715	0.30	1300 [240]	2.3	7.7	1.5	702	2300

[a] In degassed CH_2Cl_2 at 295 K, except where indicated otherwise. [b] Emission maxima and photoluminescence quantum yields Φ_{lum} determined from spectra recorded using a Synapse CCD detector. [c] Measured in deoxygenated solution, using $[Ru(bpy)_3]Cl_{2(aq)}$ as the standard. [d] Luminescence lifetimes in deoxygenated solution. Values in air-equilibrated solution are given in square parenthesis. [e] Radiative (k_r) and non-radiative (Σk_{nr}) rate constants estimated from quantum yield and lifetime, assuming unitary population of the emissive state upon light absorption: $k_r \sim \Phi / \tau$; $k_{nr} \sim (1-\Phi) / \tau$. [f] Bimolecular Stern-Volmer constant for quenching by molecular oxygen, estimated from the lifetimes in deoxygenated and air-equilibrated solution, and assuming $[O_2]$ = 2.2 mmol dm^{-3} at atmospheric

pressure of air. [g] In diethyl ether / isopentane / ethanol (2:2:1 v/v). [h] Emission spectra at 77 K were recorded using a conventional monochromator and Hamamatsu R928 PMT detector. For additional spectra, see Figure S9 and S10.

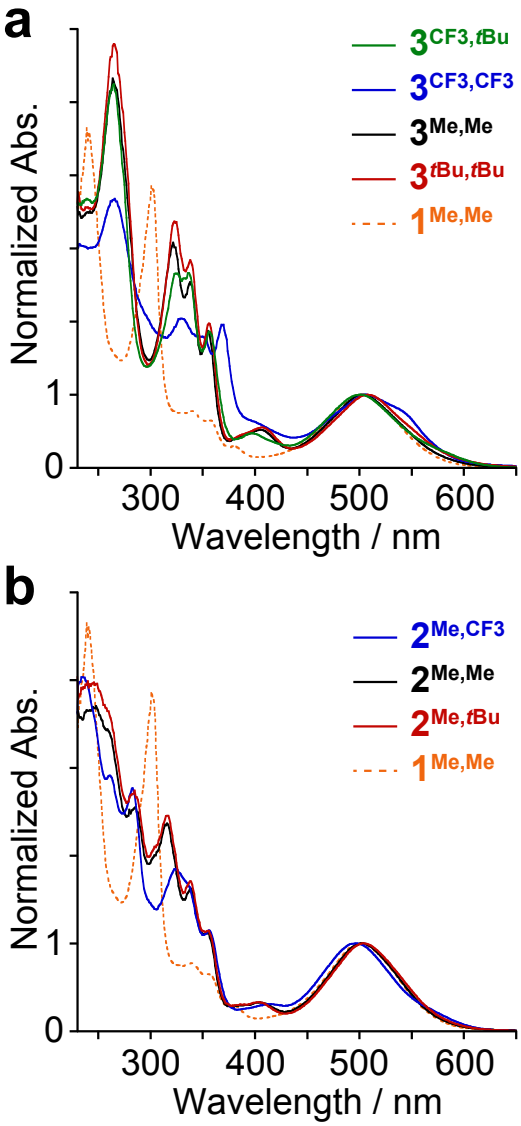

Figure 5. UV-visible absorption spectra in CH_2Cl_2 solution at 295 K of (a) *bis*(phenanthridine) series $\mathbf{3}^{\mathbf{R,R}}$; (b) three of the mixed quinoline-phenanthridine series $\mathbf{2}^{\mathbf{Me,R}}$ ($\mathbf{2}^{\mathbf{H,R}}$ are shown in Figure S9). In both panels, the absorption spectrum of the *bis*(quinoline) complex $\mathbf{1}^{\mathbf{Me,Me}}$ is provided for comparison.

DFT modeling of $\mathbf{3}^{\mathbf{CF3,CF3}}$ is consistent with this observation (Figure 6). Namely, the introduction of strongly electron-withdrawing CF_3 groups has a stabilizing influence on both the HOMO of $\mathbf{3}^{\mathbf{CF3,CF3}}$ (E_{HOMO} = -5.74 eV) compared to $\mathbf{3}^{\mathbf{Me,Me}}$ (E_{HOMO} = -5.29 eV; ΔE_{HOMO} = -0.45 eV) and the LUMO+1 (E_{LUMO+1} = -2.40 eV, $\mathbf{3}^{\mathbf{CF3,CF3}}$; E_{LUMO+1} = -1.92 eV, $\mathbf{3}^{\mathbf{Me,Me}}$; ΔE_{LUMO+1} = -

0.48 eV). As for $\mathbf{1}^{Me,Me}/\mathbf{2}^{Me,Me}/\mathbf{3}^{Me,Me}$,[38] TDDFT reveals the lowest energy absorption in $\mathbf{3}^{CF3,CF3}$ is dominated by the HOMO→LUMO+1 transition (Table S2, Figure S11). Interestingly, a consequence of the introduction of a strongly electron-withdrawing CF_3 substituent in $\mathbf{2}^{Me,CF3}$ is to turn on the HOMO→LUMO transition, which is predicted by TDDFT to have an oscillator strength comparable to that of the HOMO→LUMO+1 transition and thus contribute to the lowest energy absorption band (Table S3, Figure S12). Indeed, it appears as a low-energy shoulder in the UV-Vis absorption spectrum (Figure 5). Consequently, the broad, lowest energy absorption band for $\mathbf{2}^{Me,CF3}$ is not significantly shifted compared to the rest of the $\mathbf{2}^{R,R}$ series. Despite a larger HOMO-LUMO+1 energy gap, the participation of the lower energy HOMO→LUMO transition keeps the absorption maximum relatively unchanged.

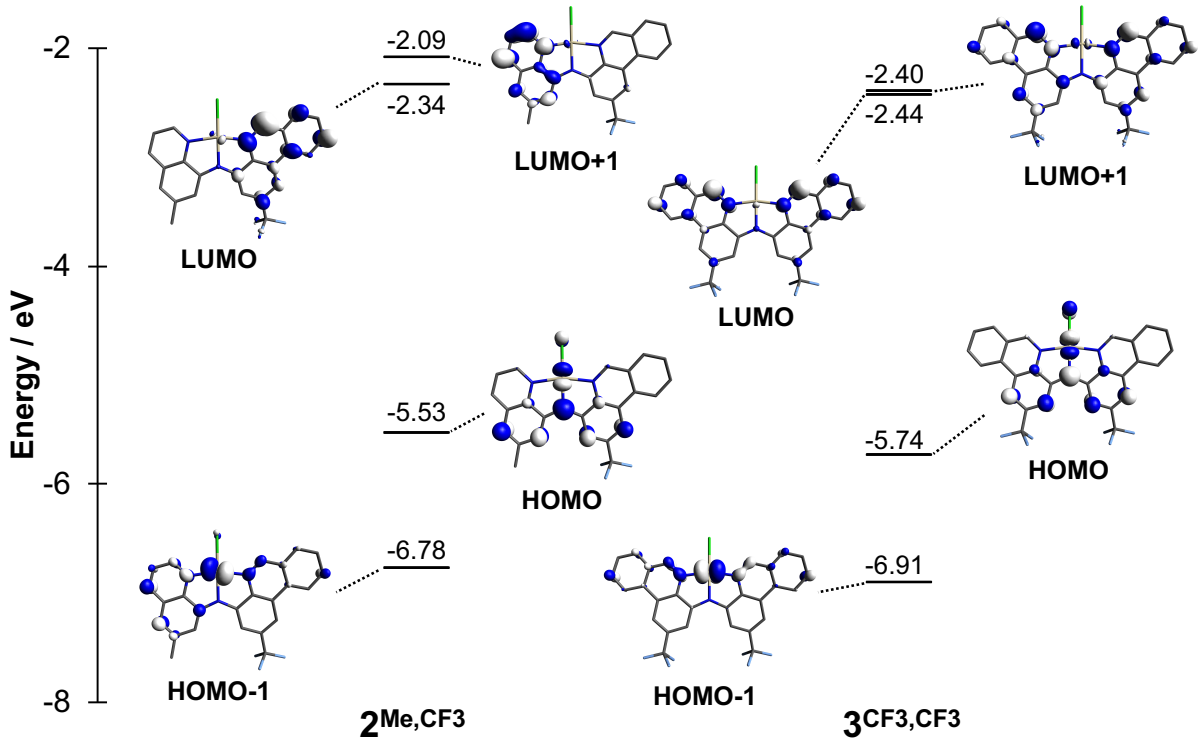

Figure 6. Selected MOs and energies (IEFPCM[CH_2Cl_2]-M06/LANL2DZ; isosurface = 0.05) of $\mathbf{2}^{Me,CF3}$ and $\mathbf{3}^{CF3,CF3}$.

The location of the CF_3 substituent on the phenanthridinyl arm in $\mathbf{2}^{Me,CF3}$ has an unequal effect on the HOMO, LUMO and LUMO+1. Specifically, the electron-withdrawing effect of CF_3 results in relatively significant stabilization of both the HOMO and LUMO compared to in $\mathbf{2}^{Me,Me}$ but has less of an impact on the acceptor LUMO+1. The influence on the HOMO can be attributed to an inductive stabilization on the amido nitrogen *meta* to the substituent. For the

mixed quin/phen systems $\mathbf{2}^{\mathbf{R,R}}$, the LUMO and LUMO+1 are comprised of different relative contributions from the quinolinyl and phenanthridinyl arms. In $\mathbf{2}^{\mathbf{Me,Me}}$, the quinolinyl moiety contributes more than the phenanthridinyl unit does to the LUMO+1 and vice versa for the LUMO.[38] Introducing a CF_3 substituent exaggerates this asymmetry, such that the phenanthridinyl arm completely dominates the LUMO in $\mathbf{2}^{\mathbf{Me,CF3}}$ (see Tables S4 and S5 for population analysis). Thus, the LUMO energy is most drastically impacted by introduction of a strongly electron-withdrawing CF_3 substituent; the LUMO+1, less so. In pseudooctahedral Fe(II) complexes of $\mathbf{L2}^{\mathbf{H,CF3}}$ and $\mathbf{L2}^{\mathbf{H,}\mathit{t}\mathbf{Bu}}$, introduction of a strongly electron-withdrawing CF_3 at the phenanthridine was found to similarly increase the phenanthridine contributions to the LUMO over those from quinoline.[44] This contrasts with what is often observed for CF_3-containing luminescent organometallics (*e.g.*, those based on cyclometallating ligands) where, although both HOMO and LUMO are stabilized, the latter is more so, largely inducing bathochromic shifts.[51,52] Structure-property relationships accounting for the placement of substituents relative to the primary orbital density comprising the HOMO and LUMO have been previously used to explain unequal impacts on the frontier orbitals in cyclometallated Ir emitters.[49] It is notable that λ_{max} for $\mathbf{2}^{\mathbf{Me,CF3}}$ is still some 27 nm red-shifted compared to $\mathbf{3}^{\mathbf{CF3,CF3}}$, which has no quinoline unit.

All twelve platinum complexes are emissive at room temperature in deoxygenated solution, with luminescence in the deep red/NIR that tails to 800–1000 nm (Figure 7, Figure S9; Table 2). Owing to the poor sensitivity of conventional photomultiplier tubes in this region, the spectra shown in Figure 7 were recorded using a CCD detector with superior sensitivity in the NIR (see Experimental Section for details). Each spectrum contains a relatively narrow, unstructured band (FWHM ~ 2300 cm^{-1}). In our initial study of the parent dimethyl complexes, we noted how emission from the *bis*(phenanthridine) complex $\mathbf{3}^{\mathbf{Me,Me}}$ is unequivocally higher in energy compared to that of the quinoline-containing complexes $\mathbf{1}^{\mathbf{Me,Me}}$ and $\mathbf{2}^{\mathbf{Me,Me}}$, in spite of the greater conjugation of the phenanthridinyl-containing ligands.[38] We traced this to enhanced rigidity within the benzannulated phenanthridinyl systems, which results in a higher energy emissive triplet state. The "mixed" system $\mathbf{2}^{\mathbf{Me,Me}}$ behaves like the *bis*(quinoline) $\mathbf{1}^{\mathbf{Me,Me}}$, implying the emissive state in both primarily involves the quinoline.

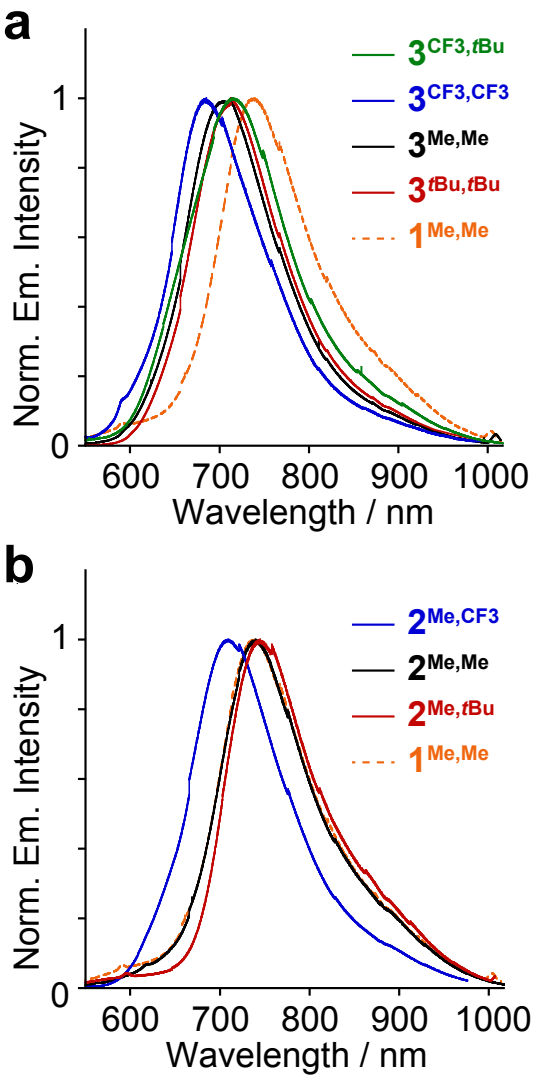

Figure 7. Photoluminescence spectra in CH_2Cl_2 at 295 K of (a) the *bis*(phenanthridine) series $\mathbf{3}^{\mathbf{R,R}}$; (b) three mixed quinoline-phenanthridine $\mathbf{2}^{\mathbf{Me,R}}$ complexes ($\mathbf{2}^{\mathbf{H,R}}$ are shown in Figure S9). In both panels, the emission spectrum of the *bis*(quinoline) complex $\mathbf{1}^{\mathbf{Me,Me}}$ is provided for comparison.

These observations are largely borne out amongst the new series of complexes, with most of the quinoline-containing compounds ($\mathbf{1}^{\mathbf{R,R}}$ and $\mathbf{2}^{\mathbf{R,R}}$) emitting at lower energy than the *bis*(phenanthridines) $\mathbf{3}^{\mathbf{R,R}}$. Within the series of substituted *bis*(phenanthridine) complexes, it can be seen that the substituents have a small but noticeable influence on λ_{max} (Figure 7a). The trend parallels that observed in the proligands. Namely, a blue shift is observed on going from the *bis*-CH_3 $\mathbf{3}^{\mathbf{Me,Me}}$ to *bis*-CF_3-substituted complex $\mathbf{3}^{\mathbf{CF3,CF3}}$, while a red shift results from introduction of *t*Bu groups in $\mathbf{3}^{\mathbf{CF3,tBu}}$ and $\mathbf{3}^{\mathbf{tBu,tBu}}$. As noted above, the introduction of strongly electron-

withdrawing CF_3 substituents in $\mathbf{3}^{\mathbf{CF3,CF3}}$ stabilizes both the HOMO and LUMO+1 by similar amounts (ΔE_{HOMO} = -0.45 eV; ΔE_{LUMO+1} = -0.48 eV). In comparison, the LUMO is stabilized by a smaller amount (ΔE_{LUMO} = -0.39 eV). This has an overall destabilizing effect on the lowest-lying emissive state [$E(T_1)$ = 2.03 eV; Table S6], which is thus less stabilized than the T_1 state of $\mathbf{3}^{\mathbf{Me,Me}}$ [$E(T_1)$ = 1.88 eV][38] resulting in blue-shifted emission despite slightly red-shifted absorption. As for $\mathbf{3}^{\mathbf{Me,Me}}$, optimization of the T_1 structure of $\mathbf{3}^{\mathbf{CF3,CF3}}$ reveals the most significant excited state distortions in the lowest-lying T_1 state are localized in the phenanthridinyl ligand arms; the coordination environment about the Pt center is left largely untouched (Table S7, Figure S13).

The "mixed" complexes in series $\mathbf{2}^{\mathbf{R,R}}$, in comparison, reveal a different picture. Those incorporating methyl or *t*Bu substituents in the phenanthridine emit at similar energy to the parent $\mathbf{2}^{\mathbf{Me,Me}}$ and $\mathbf{2}^{\mathbf{H,Me}}$, consistent the emissive excited state involving the quinoline (rather than the phenanthridine). However, emission from both $\mathbf{2}^{\mathbf{Me,CF3}}$ and $\mathbf{2}^{\mathbf{H,CF3}}$ is blue-shifted by ~30 nm relative to the rest of the $\mathbf{2}^{\mathbf{R,R}}$ series, rendering their emission maxima similar to those of some of the *bis*(phenanthridines) and apparently counteracting the red-shifting effect of the quinoline. Comparing the optimized structures of the T_1 and ground state (S_0) of $\mathbf{2}^{\mathbf{Me,CF3}}$, the most significant distortions are in fact localized in the C_5N rings of the phenanthridinyl ligand arm (Figure S13). Thus, unlike for $\mathbf{1}^{\mathbf{R,R}}$ and $\mathbf{2}^{\mathbf{R,R}}$, inclusion of strongly electron-withdrawing substituents leads to emissive excited states in the CF_3-substituted analogs with stronger participation of the phenanthridine rather than the quinoline. A plot of the spin density in the lowest lying T_1 state (Figure S14) supports this assertion and confirms the ^{3}MLCT character of the lowest lying triplet excited states for both $\mathbf{2}^{\mathbf{Me,CF3}}$ and $\mathbf{3}^{\mathbf{CF3,CF3}}$. The higher energy emission from $\mathbf{2}^{\mathbf{R,CF3}}$ can be traced to a higher energy T_1 state [$E(T_1, \mathbf{2}^{\mathbf{Me,CF3}})$ = 1.79 eV vs $E(T_1, \mathbf{2}^{\mathbf{Me,Me}})$ = 1.77 eV[38]].

In deoxygenated solutions, the observed excited-state lifetimes are on the order of a microsecond, typical of cyclometallated Pt(II) complexes (Table 2). These values are consistent with formally spin-forbidden phosphorescence from a triplet excited state, expedited by the spin-orbit coupling of the heavy metal. In air-equilibrated solutions, the lifetimes are shorter by an order of magnitude. The triplet excited state is quenched by molecular oxygen with bimolecular rate constants of ~2×10^9 M^{-1} s^{-1}. The quantum yields are all low, in the range of 0.1–0.5%. Interestingly, the complexes that display the brightest emission do not have the longest lifetimes,

suggesting that structural variation influences both radiative k_r and non-radiative k_{nr} rate constants. Assuming that the emitting state is formed with unit efficiency, these rate constants can be estimated using the expressions $k_r = \Phi / \tau$ and $k_{nr} = (\tau^{-1} - k_r)$. Considering first the k_{nr} values, it can be seen that the highest values are found for the complexes that emit at lowest energy and vice versa, as predicted by the "energy gap law". This trend is expected in the absence of deactivation processes involving higher-lying states for compounds that present a common type of excited state, as intramolecular energy transfer into vibrational modes becomes increasingly probable.[53] Previous studies of Ru(II) and Pt(II) complexes[54–56] revealed a logarithmic dependence. Here, a fairly convincing linear relationship can be seen in a plot of $\ln(k_{nr})$ versus the excited-state energy (which we estimate from λ_{max}), when considering the twelve complexes collectively (Figure 8). Inevitably, additional factors may be introduced when substituents are added that could also influence k_{nr} and cause some deviation from linearity.

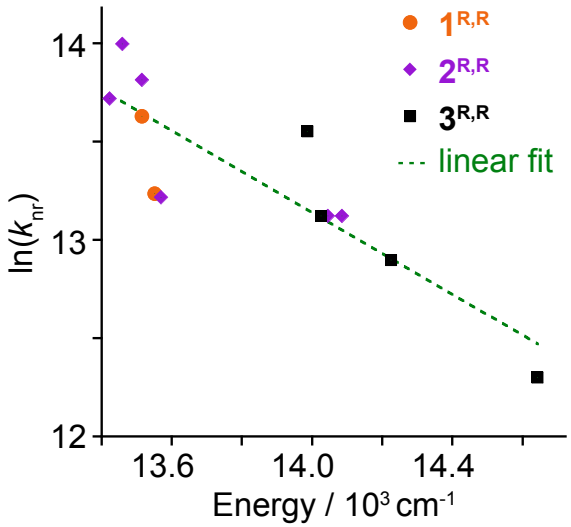

Figure 8. Plot of $\ln(k_{nr})$ versus the emission energy, estimated from $\lambda_{max,em}$ in degassed CH_2Cl_2 at 295 K. Data points for the *bis*(quinoline) complexes (**1**^{R,R}; orange circles), *bis*(phenanthridine) series (**3**^{R,R}; black squares) and the mixed quinoline-phenanthridine series (**2**^{R,R}; purple diamonds) are shown along with the best linear fit using all data points (dashed green line).

On the other hand, there is no obvious trend in k_r. However, it can be seen that k_r is smallest for the highest-energy emitters **3**^{CF3,CF3} and it is evidently for this reason that its quantum yield is not the highest amongst the series, despite having the lowest k_{nr} value. In contrast, the highest quantum yields (observed for **3**^{tBu,tBu} and **3**^{CF3,tBu}) reflect k_r values that are around an order of

magnitude larger (*e.g.*, for $\mathbf{3}^{\mathbf{CF3,CF3}}$ and $\mathbf{3}^{\mathbf{\textit{t}Bu,\textit{t}Bu}}$, the k_r values are 220 and 2400 s^{-1} respectively). Since k_r for the formally forbidden phosphorescence process is determined by the efficiency of spin-orbit coupling, which in turn is dependent on the degree of metal character in the excited state, these observations might suggest a better matching of orbital energies of ligand and metal when electron-donating substituents are present. The efficiency of spin-orbit coupling is also inversely dependent on the S_1–T_1 energy gap, and so it is possible that this gap is smallest in $\mathbf{3}^{\mathbf{\textit{t}Bu,\textit{t}Bu}}$ and $\mathbf{3}^{\mathbf{CF3,\textit{t}Bu}}$.

Although the quantum yields are low, such values are quite typical for NIR-phosphorescent complexes of many transition metals in solution where the combined effects of fast non-radiative decay and a low degree of metal participation in the excited state conspire to limit efficiency.[4,57] The best reported performance for Pt(II) systems is offered by complexes of highly conjugated benzoporphyrins, where quantum yields in excess of 50% have been observed,[4,58] but their synthesis is often demanding, with poor solubility and marked propensity to aggregation. In OLED devices, the use of bimolecular excited states formed through interfacial intermolecular interactions between Pt(II) complexes offers an alternative way of achieving efficient NIR emission,[23,29] but some of the best performing OLED emitters of this type are actually non-emissive in solution.[59] Notable features of the Pt(II) complexes reported here are the relatively narrow spectra (2300 cm^{-1} compared to > 3000 cm^{-1} for some excimer-based systems[28,29]) and the sharp onset of emission on the high-energy side of the spectrum. This latter property limits or even eliminates contamination of the spectrum by visible emission, a requirement in some applications of NIR OLEDs.

CONCLUSION

In conclusion, we present here a synthetic methodology based on chelating, pincer-like benzannulated diarylamido ligand scaffolds for constructing phosphorescent Pt(II) complexes which emit in the deep red region of the electromagnetic spectrum with narrow band profiles. The construction of 2-substituted phenanthridines amenable to cross-coupling conditions enables the preparation of a wide library of compounds, with varying substituents, as in the $\mathbf{L2}^{\mathbf{R,R}}$ and $\mathbf{L3}^{\mathbf{R,R}}$ series of proligands and platinum complexes $\mathbf{2}^{\mathbf{R,R}}$ and $\mathbf{3}^{\mathbf{R,R}}$. Benzannulation, counter-intuitively but markedly, blue-shifts emission in this series, attributable to an increase in

molecular rigidity and the ability of the phenanthridine (3,4-benzoquinoline) units to buffer against substantial molecular reorganization.[38] The influence of substituents in the phenanthridine 2-position can further be used to modulate the photophysical properties dependent on the relative strength of the substituent as an electron donating/accepting group. This influence therefore is subtle for substituents with lower Hammett parameters (Me, *t*Bu) compared to those with larger ones (CF_3).[50] Overall, the impact of CF_3 substituents is most pronounced, leading to significant hypsochromic shifts to emission, to such an extent that the $\mathbf{2}^{\mathbf{Me,CF3}}$ and $\mathbf{2}^{\mathbf{H,CF3}}$ complexes emit at higher energy than the *bis*(quinolines) $\mathbf{1}^{\mathbf{Me,Me}}$ and $\mathbf{1}^{\mathbf{H,H}}$. This influence is traced to unequal impacts of the substituent on the HOMO and LUMO+1, which represent the donor and acceptor orbitals involved in formation of the lowest energy excited state. The phosphorescence radiative rate constants of the complexes are mostly in excess of 10^3 s^{-1} but are reduced in the highest-energy emitters, possibly due to mismatching of metal and ligand orbitals and hence inefficient spin-orbit coupling. The non-radiative rate constants, meanwhile, show a trend that is in line with that expected from the energy gap law, with the lowest-energy emitters subject to the most rapid non-radiative decay. Efforts to improve deep red phosphorescence further by addressing the relative rates of radiative vs. non-radiative decay through ligand design[60] are now underway.

Experimental Section

General Information

Air-sensitive manipulations were performed in either a N_2-filled glove box or using standard Schlenk techniques in argon atmosphere. $Pd_2(dba)_3$, $Pd(PPh_3)_4$, $Pd(OAc)_2$, (±)-2,2′-*bis*(diphenylphosphino)-1,1′-binaphthalene (*rac*-BINAP), 1,1'-bis(diphenylphosphino)ferrocene (dppf), sodium *tert*-amoxide (NaO*t*Am) and sodium *tert*-butoxide (NaO*t*Bu) were purchased (Sigma Aldrich) and used without further purification. 8-Bromo-6-methylquinoline,[40] 8-amino-6-methylquinoline,[61] 4-amino-2-trifluoromethylphenanthridine,[62] $Pt(COD)Cl_2$,[63] 4-amino-2-methylphenanthridine, $\mathbf{L1}^{\mathbf{Me,Me}}$, $\mathbf{L2}^{\mathbf{Me,Me}}$, $\mathbf{1}^{\mathbf{Me,Me}}$ and $\mathbf{2}^{\mathbf{Me,Me}}$,[38] $\mathbf{L3}^{\mathbf{Me,Me}}$ and $\mathbf{3}^{\mathbf{Me,Me}}$,[43] $\mathbf{L2}^{\mathbf{H,tBu}}$ and $\mathbf{L2}^{\mathbf{H,CF3}}$ [44] were synthesized according to literature procedures. Organic solvents were dried and distilled using appropriate drying agents, and distilled water was degassed prior to use. 1- and 2D NMR spectra were recorded on Bruker Avance 300 MHz or Bruker Avance–III 500 MHz spectrometers. All ^1H and $^{13}C\{^1H\}$ NMR spectra were referenced to residual solvent peaks. ^{19}F

NMR spectra were collected using deuterated solvents and locked to the deuterium signal. NMR spectra of all new compounds are provided in Figures S15-S39. Elemental analyses were performed by Microanalytical Service Ltd., Delta, BC (Canada), and at the University of Manitoba using a Perkin Elmer 2400 Series II CHNS/O Elemental Analyzer.

Synthesis of Ligand Precursors

4-bromo-2-*tert*-butylphenanthridine: A 500 mL Teflon-stoppered flask was charged with $Pd(PPh_3)_4$ (1.66 g, 1.43 mmol) and 50 mL of 1,2-dimethoxyethane (DME). After stirring briefly to mix, 2-bromo-6-iodo-4-*tert*-butyl-toluidine (15.02 g, 47.80 mmol), 2-formylphenylboronic acid (7.89 g, 52.58 mmol) and an additional 70 mL of DME were added, followed by Na_2CO_3 (15.20 g, 143.4 mmol) dissolved in 100 mL of degassed water. The flask was then sealed, and the mixture stirred vigorously for 6 h in an oil bath (130 °C). The flask was then allowed to cool, $HCl_{(aq)}$ (2 M, 130 mL) added, and the mixture refluxed for additional 2 h. The flask was then cooled, neutralized with NaOH, and pumped to dryness. The residue was taken up in CH_2Cl_2 (100 mL) and washed with brine (3 × 100 mL). The organic layer was separated, dried over Na_2SO_4 and volatiles removed to leave a yellow-brown solid. Column chromatography on basic alumina gave a pale-yellow solid (R_f = 0.41; 1:5 EtOAc/hexane). Isolated yield = 11.74 g (86 %). ^{1}H NMR ($CDCl_3$, 500 MHz, 22 °C): δ 9.33 (s, 1H; $C_{Ar}H$), 8.62 (d, 1H, J_{HH} = 8.4 Hz; $C_{Ar}H$), 8.52 (s, 1H; $C_{Ar}H$), 8.14 (d, 1H, J_{HH} = 1.9 Hz; $C_{Ar}H$), 8.06 (d, 1H, J_{HH} = 7.9 Hz; $C_{Ar}H$), 7.87 (t, 1H, J_{HH} = 7.6 Hz; $C_{Ar}H$), 7.71 (t, 1H, J_{HH} = 7.4 Hz; $C_{Ar}H$), 1.49 ppm (s, 9H; *t*Bu). $^{13}C\{^1H\}$ NMR ($CDCl_3$, 125 MHz, 22 °C): δ 153.8 (C_{Ar}), 150.9 (C_{Ar}), 140.0 (C_{Ar}), 132.6 (C_{Ar}), 131.3 (C_{Ar}), 131.1 (C_{Ar}), 129.1 (C_{Ar}), 128.0 (C_{Ar}), 126.6 (C_{Ar}), 125.5 (C_{Ar}), 125.3 (C_{Ar}), 122.0 (C_{Ar}), 117.8 (C_{Ar}), 35.4 (CCH_3)$_3$, 31.5 ppm (CH_3).

General Procedure for Proligand Synthesis (L1-L3):

A thick-walled, 100 mL Teflon-stoppered flask was charged with a Pd catalyst, ligand (*rac*-BINAP or dppf) and toluene (30 mL) in the amounts noted below. After stirring briefly, the appropriate quinoline or phenanthridine reagents were added, along with an additional 30 mL of toluene, followed by the alkoxide base. The sealed flask was then stirred vigorously for 72 h in an oil bath set to 150 °C. After cooling and removing the volatiles, the residue was taken up in CH_2Cl_2 (120 mL) with the resulting suspension filtered over Celite and dried.

L2^{Me,tBu}: The general procedure was followed using: $Pd_2(dba)_3$ (0.110 mg, 0.120 mmol), *rac*-BINAP (0.162 g, 0.440 mmol); 8-bromo-6-methylquinoline (0.490 g, 2.20 mmol), 4-amino-2-*tert*-butylphenanthridine (0.500 g, 2.00 mmol); and NaO*t*Am (0.29 g, 3.0 mmol). Column chromatography gave an orange-red solid (neutral alumina; 1:5 EtOAc/hexane; R_f = 0.43). Isolated yield = 1.01 g (92%). ^{1}H NMR ($CDCl_3$, 300 MHz, 22 °C): δ 10.43 (br s, 1H; N*H*), 9.29 (s, 1H; $C_{Ar}H$), 8.91 (dd, 1H, J_{HH} = 4.2, 1.7 Hz; $C_{Ar}H$), 8.68 (d, 1H, J_{HH} = 8.2; $C_{Ar}H$), 8.19-8.02 (m, 4H; $C_{Ar}H$), 7.91-7.82 (m, 1H; $C_{Ar}H$), 7.77 (d, 1H, J_{HH} = 1.6 Hz; $C_{Ar}H$), 7.70 (dd, 1H, J_{HH} = 8.0, 7.0 Hz; $C_{Ar}H$), 7.46-7.39 (m, 1H; $C_{Ar}H$), 7.11 (br s, 1H; $C_{Ar}H$), 2.57 (s, 3H; CH_3), 1.57 (s, 9H, C(CH_3)$_3$ ppm. ^{13}C{^{1}H} NMR ($CDCl_3$, 75 MHz, 22 °C): δ 150.6 (C_{Ar}), 150.4 (C_{Ar}), 147.3 (C_{Ar}), 139.2 (C_{Ar}), 139.0 (C_{Ar}), 137.0 (C_{Ar}), 135.5 (C_{Ar}), 133.1 (C_{Ar}), 130.7 (C_{Ar}), 129.2 (C_{Ar}), 128.9 (C_{Ar}), 127.3 (C_{Ar}), 127.0 (C_{Ar}), 124.3 (C_{Ar}), 122.4 (C_{Ar}), 121.8 (C_{Ar}), 116.7 (C_{Ar}), 111.6 (C_{Ar}), 110.9 (C_{Ar}), 108.8 (C_{Ar}), 35.7(C(CH$_3$)$_3$), 31.7 (^{Phen}CH$_3$), 22.7 (^{Quin}CH$_3$) ppm.

L2^{Me,CF3}: The general procedure was followed using: $Pd(OAc)_2$ (0.025 g, 0.11 mmol), dppf (0.086 g, 0.15 mmol); 4-bromo-2-trifluoromethylphenanthridine (0.710 g, 2.18 mmol), 8-amino-6-methylquinoline (0.350 g, 2.23 mmol); and NaO*t*Am (0.35 g, 3.27 mmol). Column chromatography gave a yellow-green solid (neutral alumina; 1:5 EtOAc/hexane; R_f = 0.3). Isolated yield = 0.77 g (88%). ^{1}H NMR ($CDCl_3$, 300 MHz, 22 °C): δ 10.74 (br s, 1H; N*H*), 9.43 (s, 1H; $C_{Ar}H$), 8.90 (dd, 1H, J_{HH} = 4.1, 1.7 Hz; $C_{Ar}H$), 8.65 (d, 1H, J_{HH} = 8.5 Hz; $C_{Ar}H$), 8.32 (s, 1H; $C_{Ar}H$), 8.18-8.04 (overlapped m, 3H; $C_{Ar}H$), 7.93 (dd, J_{HH} = 8.4, 7.1 Hz; 1H, $C_{Ar}H$), 7.83-7.73 (overlapped m, 2H; $C_{Ar}H$), 7.45 (dd, 1H, J_{HH} = 8.3, 4.2 Hz; $C_{Ar}H$), 7.23-7.14 (br s, 1H; $C_{Ar}H$), 2.60 ppm (s, 3H; $_{Quin}$CH_3). ^{13}C{^{1}H} NMR ($CDCl_3$, 75 MHz, 22 °C): δ 153.0 (C_{Ar}), 147.6 (C_{Ar}), 140.7 (C_{Ar}), 139.1 (C_{Ar}), 137.9 (C_{Ar}), 137.2 (C_{Ar}), 136.4 (C_{Ar}), 135.6 (C_{Ar}), 132.9 (C_{Ar}), 131.6 (C_{Ar}), 131.0 (q, C_{Ar}), 129.6 (C_{Ar}), 129.20 (C_{Ar}), 129.16 (C_{Ar}), 128.3 (C_{Ar}), 127.1 (C_{Ar}), 124.5 (C_{Ar}), 122.6 (C_{Ar}),122.0 (C_{Ar}), 118.2 (C_{Ar}), 113.1 (C_{Ar}), 109.6 (q, C_{Ar}), 106.0 (q, C_{Ar}), 22.6 ppm ($_{Quin}$CH$_3$). ^{19}F{^{1}H} NMR ($CDCl_3$, 282 MHz, 22 °C): δ -62.26 ppm.

L3^{tBu,tBu}: The general procedure was followed using: $Pd(OAc)_2$ (0.032 g, 0.14 mmol); dppf (0.13 g, 0.23 mmol); 4-bromo-2-*tert*-butylphenanthridine (0.90 g, 2.9 mmol); 4-amino-2-*tert*-butylphenanthridine (0.70 g, 3.2 mmol); and NaO*t*Am (0.45 g, 4.3 mmol). Column chromatography gave a yellow-green solid (neutral alumina; 1:5 EtOAc/hexane; R_f = 0.35). Isolated yield = 1.08 g (78%). ^{1}H NMR ($CDCl_3$, 300 MHz, 22 °C): δ 10.41 (br s, 1H; N*H*), 9.30

(s, 2H; $C_{Ar}H$), 8.69 (d, 2H, J_{HH} = 8.4 Hz; $C_{Ar}H$), 8.18 (s, 2H; $C_{Ar}H$), 8.14-8.05 (overlapped m, 4H; $C_{Ar}H$), 7.91-7.82 (m, 2H; $C_{Ar}H$), 7.76 (m, 2H; $C_{Ar}H$), 1.55 ppm (s, 18H; $C(CH_3)_3$). $^{13}C\{^1H\}$ NMR ($CDCl_3$, 75 MHz, 22 °C): δ 150.54 (C_{Ar}), 150.50 (C_{Ar}), 139.7 (C_{Ar}), 134.0 (C_{Ar}), 133.2 (C_{Ar}), 130.7 (C_{Ar}), 128.9 (C_{Ar}), 127.3 (C_{Ar}), 127.1 (C_{Ar}), 124.4 (C_{Ar}), 122.4 (C_{Ar}), 110.0 (C_{Ar}), 108.5 (C_{Ar}), 35.7 ($C(CH_3)_3$), 31.8 ppm ($C(CH_3)_3$).

L3^{CF3,CF3}: The general procedure was followed using: $Pd(OAc)_2$ (21.0 mg, 0.09 mmol); dppf (72.0 mg, 0.13 mmol); 4-bromo-trifluoromethylphenanthridine (0.65 g, 1.99 mmol); 4-amino-2-trifluoromethylphenanthridine (0.53 g, 2.33 mmol); and NaO*t*Am (0.29 g, 2.78 mmol). Column chromatography gave a yellow-green solid (neutral alumina; 1:5 EtOAc/hexane; R_f = 0.2). Isolated yield = 0.76 g (74%). ^1H NMR ($CDCl_3$, 500 MHz, 22 °C): δ 10.91 (br s, 1H, N-*H*), 9.42 (s, 2H, $C_{Ar}H$), 8.63 (d, 2H, J_{HH} = 8.1 Hz, $C_{Ar}H$), 8.34 (s, 2H, $C_{Ar}H$), 8.20-8.08 (overlapped m, 4H, $C_{Ar}H$), 7.94 (app t, J_{HH} = 7.4 Hz, 2H, $C_{Ar}H$), 7.83 ppm (app t, 2H, J_{HH} = 7.3 Hz, $C_{Ar}H$). $^{13}C\{^1H\}$ NMR ($CDCl_3$, 125 MHz, 22 °C): δ 153.3 (C_{Ar}), 140.0 (C_{Ar}), 136.5 (C_{Ar}), 132.8 (C_{Ar}), 131.8 (C_{Ar}), 129.23 (C_{Ar}), 129.19 (C_{Ar}), 128.5 (C_{Ar}), 128.4 (C_{Ar}), 127.1 (C_{Ar}), 124.7 (C_{Ar}), 122.6 (C_{Ar}), 110.7 (C_{Ar}), 106.7 ppm (C_{Ar}). $^{19}F\{^1H\}$ NMR ($CDCl_3$, 470 MHz): δ -62.45 ppm.

L3^{CF3,tBu}: The general procedure was followed using: $Pd(OAc)_2$ (0.025 g, 0.11 mmol), dppf (0.083 g, 0.15 mmol); 4-bromo-2-trifluoromethylphenanthridine (0.70 g, 2.2 mmol); 4-amino-2-*tert*-butylphenanthridine (0.55 g, 2.2 mmol); and NaO*t*Am (0.34 g, 3.2 mmol). Column chromatography gave a yellow-green solid (neutral alumina; 1:5 EtOAc/hexane; R_f = 0.32). Isolated yield = 0.89 g (83%) ^1H NMR ($CDCl_3$, 300 MHz, 22 °C): δ 10.57 (br s, 1H; N*H*), 9.43 (s, 1H; $C_{Ar}H$), 9.30 (s, 1H; $C_{Ar}H$), 8.67 (dd, 2H, J_{HH} = 11.7, 8.3 Hz; $C_{Ar}H$), 8.29 (s, 1H; $C_{Ar}H$), 8.22-8.04 (m, 5H; $C_{Ar}H$), 7.97-7.85 (m, 2H; $C_{Ar}H$), 7.82-7.70 (m, 2H; $C_{Ar}H$), 1.56 ppm (s, 9H; $C(CH_3)_3$). $^{13}C\{^1H\}$ NMR ($CDCl_3$, 75 MHz, 22 °C): δ 152.9 (C_{Ar}), 151.0 (C_{Ar}), 150.6 (C_{Ar}), 141.2 (C_{Ar}), 138.5 (C_{Ar}), 136.3 (C_{Ar}), 134.3 (C_{Ar}), 133.1 (C_{Ar}), 132.9 (C_{Ar}), 131.6 (C_{Ar}), 130.9 (C_{Ar}), 129.6 (C_{Ar}), 129.2 (C_{Ar}), 129.2 (C_{Ar}), 129.0 (C_{Ar}), 128.3 (C_{Ar}), 127.5 (C_{Ar}), 127.1 (C_{Ar}), 127.1 (C_{Ar}), 124.7 (C_{Ar}), 124.5 (C_{Ar}), 122.6 (C_{Ar}), 122.4 (C_{Ar}), 111.7 (C_{Ar}), 110.0 (C_{Ar}), 109.2 (q, C_{Ar}), 105.8 (q, C_{Ar}), 35.7 ($C(CH_3)_3$), 31.6 ppm ($C(CH_3)_3$). $^{19}F\{^1H\}$ NMR ($CDCl_3$, 282 MHz, 22 °C): δ -62.52 ppm.

General Procedure for Pt Complex Synthesis: In a thick-walled Teflon-stoppered flask, equimolar amounts of $Pt(COD)Cl_2$ and NaO*t*Bu were added to a solution of the appropriate

ligand (**L1**^{R,R}, **L2**^{R,R} or **L3**^{R,R}) in CH_2Cl_2 (10 mL), and the mixture stirred vigorously in an oil bath set to 70 °C for 18 h. The resulting red suspension was allowed to cool, and the volatiles were removed *in vacuo*. The residue was then washed with acetonitrile (3 × 10 mL) and diethylether (3 × 10 mL).

2^{H,tBu}**:** The general procedure was followed using: **L2**^{H,tBu} (0.20 g, 0.53 mmol), Pt(COD)Cl_2 (0.20 g, 0.54 mmol), and NaO*t*Bu (0.050 g, 0.54 mmol). Isolated yield = 0.279 g (87%). ^{1}H NMR ($CDCl_3$, 300 MHz, 22 °C): δ 9.60 (s, 1H, $^3J_{PtH}$ = 39 Hz, $C_{Ar}H$), 9.25 (d, 1H, J_{HH} = 5.0 Hz; $C_{Ar}H$), 8.58 (d, 1H, J_{HH} = 8.4 Hz; $C_{Ar}H$), 8.27 (d, 1H, J_{HH} = 8.2 Hz; $C_{Ar}H$), 8.09 (d, 1H, J_{HH} = 8.0 Hz; $C_{Ar}H$), 8.03-7.85 (overlapped m, 2H, $C_{Ar}H$), 7.80 (s, 1H, $C_{Ar}H$), 7.76-7.68 (overlapped m, 2H, $C_{Ar}H$), 7.53 (app t, 1H, J_{HH} = 8.0 Hz; $C_{Ar}H$), 7.41 (dd, 1H, J_{HH} = 8.3, 5.0 Hz; $C_{Ar}H$), 7.06 (d, 1H, J_{HH} = 7.9 Hz; $C_{Ar}H$), 1.57 ppm (s, 9H, CH_3). Anal. Calcd for $C_{26}H_{22}ClN_3Pt$: C, 51.45; H, 3.65. Found: C, 51.15; H, 3.74.

2^{H,CF3}**:** The general procedure was followed using: **L2**^{H,CF3} (0.10 g, 0.26 mmol), Pt(COD)Cl_2 (0.096 g, 0.26 mmol), and NaO*t*Bu (0.026 mg, 0.27 mmol). Isolated yield = 0.279 g (87%). ^{1}H NMR ($CDCl_3$, 500 MHz, 22 °C): δ 9.79 (s, 1H, $C_{Ar}H$), 9.30 (d, 1H, J_{HH} = 5.4 Hz; $C_{Ar}H$), 8.59 (d, 1H, J_{HH} = 8.6 Hz; $C_{Ar}H$), 8.36 (d, 1H, J_{HH} = 8.4 Hz; $C_{Ar}H$), 8.19 (d, 1H, J_{HH} = 7.7 Hz; $C_{Ar}H$), 8.07-7.99 (overlapped m, 2H, $C_{Ar}H$), 7.94 (s, 1H, $C_{Ar}H$), 7.86-7.78 (m, 2H, $C_{Ar}H$), 7.60 (app t, 1H, J_{HH} = 7.9 Hz; $C_{Ar}H$), 7.51-7.44 (overlapped m, 1H, $C_{Ar}H$), 7.21 ppm (d, 1H, J_{HH} = 8.0 Hz; $C_{Ar}H$). ^{19}F{^{1}H} NMR ($CDCl_3$, 470 MHz, 22 °C): δ -62.19 ppm. Anal. Calcd for $C_{23}H_{13}ClF_3N_3Pt$: C, 44.64; H, 2.12. Found: C, 44.57; H, 2.29.

2^{Me,tBu}**:** The general procedure was followed using: **L2**^{Me,tBu} (0.20 g, 0.58 mmol), Pt(COD)Cl_2 (0.22 g, 0.59 mmol), and NaO*t*Bu (0.06 g, 0.60 mmol). Isolated yield = 0.266 g (79%). ^{1}H NMR ($CDCl_3$, 300 MHz, 22 °C): δ 9.60 (s, 1H, $^3J_{PtH}$ = 39 Hz, $C_{Ar}H$), 9.17 (d, 1H, J_{HH} = 6.9 Hz; $C_{Ar}H$), 8.59 (d, 1H, J_{HH} = 8.2 Hz; $C_{Ar}H$), 8.17 (d, 1H, J_{HH} = 8.4 Hz; $C_{Ar}H$), 8.10 (d, 1H, J_{HH} = 7.4 Hz; $C_{Ar}H$), 7.99-7.89 (overlapped multiplet, 2H, $C_{Ar}H$), 7.80 (s, 1H, $C_{Ar}H$), 7.72 (app t, 1H, J_{HH} = 6.6 Hz; $C_{Ar}H$), 7.56 (s, 1H, $C_{Ar}H$), 7.37 (dd, 1H, J_{HH} = 8.4, 5.2 Hz; $C_{Ar}H$), 6.88 (s, 1H, $C_{Ar}H$), 2.60 (s, 3H, CH_3), 1.57 ppm (s, 9H, $C(CH_3)_3$). Anal. Calcd for $C_{27}H_{24}ClN_3Pt$: C, 52.22; H, 3.90. Found: C, 51.91; H, 4.16.

$2^{Me,CF3}$: The general procedure was followed using: **$L2^{Me,CF3}$** (0.21 g, 0.53 mmol), $Pt(COD)Cl_2$ (0.20 g, 0.53 mmol), and NaO*t*Bu (0.05 g, 0.54 mmol). Isolated yield = 0.222 g (66%). ^1H NMR ($CDCl_3$, 300 MHz, 22 °C): δ 9.76 (s, 1H, $^3J_{PtH}$ = 39 Hz, $C_{Ar}H$), 9.18 (d, 1H, J_{HH} = 5.1 Hz; $C_{Ar}H$), 8.56 (d, 1H, J_{HH} = 8.4 Hz; $C_{Ar}H$), 8.23 (d, 1H, J_{HH} = 8.8 Hz; $C_{Ar}H$), 8.17 (d, 1H, J_{HH} = 8.0 Hz; $C_{Ar}H$), 8.08-7.95 (overlapped m, 2H, $C_{Ar}H$), 7.91 (s, 1H, $C_{Ar}H$), 7.81 (app t, 1H, J_{HH} = 7.6 Hz; $C_{Ar}H$), 7.58 (s, 1H, $C_{Ar}H$), 7.41 (dd, 1H, J_{HH} = 8.3, 5.1 Hz; $C_{Ar}H$), 7.00 (s, 1H, $C_{Ar}H$), 2.63 ppm (s, 3H, CH_3). $^{19}F\{^1H\}$ NMR ($CDCl_3$, 470 MHz, 22 °C): δ -62.49 ppm. Anal. Calcd for $C_{24}H_{15}ClF_3N_3Pt$: C, 45.54; H, 2.39. Found: C, 45.73; H, 2.41.

$3^{tBu,tBu}$: The general procedure was followed using: **$L3^{tBu,tBu}$** (0.20 g, 0.41 mmol), $Pt(COD)Cl_2$ (0.16 g, 0.42 mmol), and NaO*t*Bu (0.04 g, 0.43 mmol). Isolated yield = 0.228 g (78%). ^1H NMR ($CDCl_3$, 300 MHz, 22 °C): δ 9.63 (s, 2H, $C_{Ar}H$), 8.57 (d, 2H, J_{HH} = 8.6 Hz; $C_{Ar}H$), 8.11 (d, 2H, J_{HH} = 8.0 Hz; $C_{Ar}H$), 8.06 (s, 2H, $C_{Ar}H$), 7.99-7.88 (m, 2H, $C_{Ar}H$), 7.78 (s, 2H, $C_{Ar}H$), 7.76-7.66 (m, 2H, $C_{Ar}H$), 1.53 ppm (s, 18H, $C(CH_3)_3$). Anal. Calcd for $C_{34}H_{32}ClN_3Pt•(4xCHCl_3)(0.5xEt_2O)$: C, 44.08; H, 4.16. Found: C, 44.05, 4.26.

$3^{CF3,tBu}$: The general procedure was followed using: **$L3^{CF3,tBu}$** (0.20 g, 0.40 mmol), $Pt(COD)Cl_2$ (0.15 g, 0.41 mmol), and NaO*t*Bu (0.04 g, 0.42 mmol). Isolated yield = 0.182 g (62%). ^1H NMR ($CDCl_3$, 300 MHz, 22 °C): δ 9.75 (s, 1H, $C_{Ar}H$), 9.58 (s, 1H, $C_{Ar}H$), 8.56 (d, 1H, J_{HH} = 8.4 Hz; $C_{Ar}H$), 8.47 (d, 1H, J_{HH} = 8.4 Hz; $C_{Ar}H$), 8.16 (d, 1H, J_{HH} = 7.4 Hz; $C_{Ar}H$), 8.10 (d, 1H, J_{HH} = 8.0 Hz; $C_{Ar}H$), 8.03-7.65 (m, 8H, $C_{Ar}H$), 1.59 ppm (s, 9H, $C(CH_3)_3$). $^{19}F\{^1H\}$ NMR ($CDCl_3$, 470 MHz, 22 °C): δ -62.50 ppm. Anal. Calcd for $C_{31}H_{23}ClF_3N_3Pt$: C, 51.35; H, 3.20. Found: C, 51.43; H, 3.21.

$3^{CF3,CF3}$: The general procedure was followed using: **$L3^{CF3,CF3}$** (0.28 g, 0.54 mmol), $Pt(COD)Cl_2$ (0.21g, 0.55 mmol), and NaO*t*Bu (0.05 g, 0.56 mmol). Isolated yield of **$3^{CF3,CF3}$** = 0.265 g (66%). $^{19}F\{^1H\}$ NMR (DMSO, 470 MHz, 22 °C): δ -60.77 ppm. The compound appears to be too insoluble to characterize. Anal. Calcd for $C_{28}H_{14}ClF_3N_3Pt(2xCHCl_3)$: C, 36.93; H, 1.65. Found: C, 37.224; 1.884.

X-Ray Crystallography

X-ray crystal structure data were collected from multi-faceted crystals of suitable size and quality selected from a representative sample of crystals of the same habit using an optical

microscope. In each case, crystals were mounted on MiTiGen loops and data collection carried out in a cold stream of nitrogen (150 K; Bruker D8 QUEST ECO; Mo K_α radiation). All diffractometer manipulations were carried out using Bruker APEX3 software.[64] Structure solution and refinement was carried out using XS, XT and XL software, embedded within the Bruker SHELXTL suite.[65] For each structure, the absence of additional symmetry was confirmed using ADDSYM incorporated in the PLATON program.[66] CCDC Nos. 1992330-1992332 contain the supplementary crystallographic data for this paper. The data can be obtained free of charge from The Cambridge Crystallographic Data Center via www.ccdc.cam.ac.uk/structures.

Crystal structure data for **L3^{CF3,CF3}** (CCDC 1992332): X-ray quality crystals were grown from reaction mixture in toluene. Crystal structure parameters: $C_{28}H_{15}N_3F_6$ 507.43 g/mol, monoclinic, space group $P2_1/n$; a = 13.0578(6) Å, b = 9.2399(4) Å, c = 19.4731(10) Å, α = 90°, β = 109.319(2)°, γ = 90°, V = 2217.19(18) Å^3; Z = 4, ρ_{calcd} = 1.520 g cm^{-3}; crystal dimensions 0.22 x 0.14 x 0.06 mm^3; θ_{max} = 27.525°; 39662 reflections, 3800 independent (R_{int} = 0.0517), direct methods; absorption coeff (μ = 0.126 mm^{-1}), absorption correction semi-empirical from equivalents (SADABS); refinement (against F_o^2) with SHELXTL V6.1, 334 parameters, 0 restraints, R_1 = 0.0579 ($I > 2\sigma$) and wR_2 = 0.1518 (all data), Goof = 1.067, residual electron density 0.74/−0.55 e Å^{-3}.

Crystal structure data for **2^{Me,tBu}** (CCDC 1992330): X-ray quality crystals were grown following diffusion of diethylether vapor into a $CHCl_3$ solution of the compound at room temperature. Crystal structure parameters: $C_{27}H_{24}Cl_1N_3Pt_1$ 621.03 g/mol, triclinic, space group P-1; a = 8.8827(6)Å, b = 11.5775(8) Å, c = 12.2098(9) Å, α = 63.521(2)°, β = 77.693(2)°, γ = 88.681(2)°, V = 1094.37(13) Å^3; Z = 2, ρ_{calcd} = 1.885 g cm^{-3}; crystal dimensions 0.330 x 0.140 x 0.040 mm^3; θ_{max} = 27.916°; 27804 reflections, 5201 independent (R_{int} = 0.0288), direct methods; absorption coeff (μ = 6.554 mm^{-1}), absorption correction semi-empirical from equivalents (SADABS); refinement (against F_o^2) with SHELXTL V6.1, 293 parameters, 0 restraints, R_1 = 0.0151 ($I > 2\sigma$) and wR_2 = 0.0357 (all data), Goof = 1.057, residual electron density 0.909/−0.692 e Å^{-3}.

Crystal structure data for **3^{tBu,tBu}** (CCDC 1992331): X-ray quality crystals were grown following diffusion of diethylether vapor into a CH_2Cl_2 solution of the compound at room temperature.

Crystal structure parameters: $C_{34}H_{26}Cl_1N_3Pt_1.CH_2Cl_2$ 792.04 g/mol, orthorhombic, space group *Pnma*; a = 24.9983(13) Å, b = 6.7957(3) Å, c = 18.1591(9) Å, α = 90°, β = 90°, γ = 90°, V = 3084.9(3) Å^3; Z = 4, ρ_{calcd} = 1.705 g cm^{-3}; crystal dimensions 0.100 x 0.022 x 0.021 mm^3; θ_{max} = 24.789°; 76058 reflections, 2888 independent (R_{int} = 0.2484), direct methods; absorption coeff (μ = 4.838 mm^{-1}), absorption correction semi-empirical from equivalents (SADABS); refinement (against F_o^2) with SHELXTL V6.1, 249 parameters, 0 restraints, R_1 = 0.0461 ($I > 2\sigma$) and wR_2 = 0.0834 (all data), Goof = 1.145, residual electron density 1.273/−0.901 e Å^{-3}.

Optical Spectroscopy Measurements

The absorption spectra of the complexes were measured in solution in CH_2Cl_2 in 1 cm quartz cuvettes using a Biotek Instruments XS UV-Visible spectrometer at room temperature. The emission spectra of the proligands at 295 and 77 K, and of their Pt(II) complexes at 77 K, were recorded using a Jobin Yvon Fluoromax-2 spectrometer equipped with a red-sensitive Hamamatsu R928 photomuliplier tube. The emission spectra of the Pt(II) complexes at 295 K, which extend up to around 1000 nm, were recorded using a thermoelectrically cooled Synapse CCD detector, which offers better sensitivity in the red / NIR region compared to the R928 PMT. The samples for measurements at 295 K were contained within 1 cm pathlength quartz cuvettes modified for attachment to a vacuum line, and were degassed prior to measurement by a minimum of three freeze-pump-thaw cycles; final vapor pressure at 77 K was < 10^{-2} mbar. Emission spectra at 77 K were recorded in 4 mm diameter tubes held within a liquid nitrogen cooled quartz dewar. Luminescence lifetimes were measured by time-correlated single-photon counting (TCSPC) following excitation using a pulsed laser diode at 405 nm; the emitted light was detected at right angles to the excitation beam, using an R928 PMT thermoelectrically cooled to –20 °C.

Calculations

DFT optimizations of $\mathbf{2}^{\mathbf{Me,CF3}}$ and $\mathbf{3}^{\mathbf{CF3,CF3}}$ were carried out using Gaussian16, rev. C01[67] with M06/LANL2DZ[68,69] with an IEFPCM[70] solvent model with CH_2Cl_2. TD-DFT and single point calculations were performed at the same level of theory. Molecular orbital analyses were carried out using the Hirshfeld partition method[71] available in Multiwfn software[72] and visualized using Avogadro.[73] TD-DFT results were analyzed using GaussSum.[74] Spin density maps were

generated using Gabedit.[75] To calculate ground-state, excited-state and reorganization energies, the following protocol (Figure S40) was followed: (1) The S_0 geometry was optimized by restricted DFT (charge = 0, multiplicity = 1) using the crystal structure coordinates as starting input. The T_1 geometry was optimized with unrestricted DFT (charge = 0, multiplicity = 3) using the optimized S_0 geometry as starting input. Frequency calculations were then subsequently carried out to confirm that these structures are at a minimum. (2) To determine the relative molecular fragment contributions to the frontier MOs, population analyses were carried out on the optimized structures of S_0 states (Tables S6 and S7). The electronic energies, $E(S_0)$ and $E(T_1)$, obtained from the single point calculations of S_0 and T_1 in their respective minimum were used to estimate the adiabatic energy (E^{adia}), where, $E^{adia} = E(T_1) - E(S_0)$. (3) TD-DFT was then carried out on the first 50 $S_n \leftarrow S_0$ singlet-singlet transitions with the restricted formalism with charge = 0 and multiplicity = 1 to yield $E^{vert\text{-}abs}$. (4) $E^{vert\text{-}phos}$ ($T_1 \rightarrow T_1@S_0$) was estimated as the ΔSCF between single point energies of the T_1 (charge = 0, multiplicity = 3) and $T_1@S_0$ (charge = 0, multiplicity = 1) both at the optimized T_1 geometry.

ASSOCIATED CONTENT

Supporting Information. Packing diagrams of the X-ray structures; additional UV-Vis absorption and emission spectra; computational data tables; multi-nuclear NMR spectra of all new compounds; crystallographic information files containing all X-ray data. CCDC 1992330-1992332 contain the supplementary crystallographic data for this paper. The data can be obtained free of charge from The Cambridge Crystallographic Data Center via www.ccdc.cam.ac.uk/structures.

The following files are available free of charge:
Supporting Information File (PDF)
Combined Crystallographic Information File (CIF)

AUTHOR INFORMATION

Corresponding Authors

David E. Herbert (david.herbert@umanitoba.ca)
J. A. Gareth Williams (j.a.g.williams@durham.ac.uk)

ORCIDs

Pavan Mandapati: 0000-0002-3686-4850

Jason D. Braun: 0000-0002-5850-8048

Issiah B. Lozada: 0000-0002-1689-2918

J. A. Gareth Williams: 0000-0002-4688-3000

David E. Herbert: 0000-0001-8190-2468

Author Contributions

The manuscript was written through contributions of all authors. All authors have given approval to the final version of the manuscript.

Conflicts of Interest

There are no conflicts of interest to declare.

ACKNOWLEDGMENTS

The following sources of funding are gratefully acknowledged: Natural Sciences Engineering Research Council of Canada for a Discovery Grant to DEH (RGPIN-2014-03733); the Canadian Foundation for Innovation and Research Manitoba for an award in support of an X-ray diffractometer (CFI #32146); the University of Manitoba for a UMGF PhD Fellowship (JDB), the Bert & Lee Friesen Graduate Scholarship (IBL) and GETS support (PM, IBL and JDB). The Association of Commonwealth Universities (ACU) is thanked for a University of Manitoba Titular Fellowship (2016–17) to JAGW.

REFERENCES

(1) Li, J.; Yan, J.; Wen, D.; Khan, W. U.; Shi, J.; Wu, M.; Su, Q.; Tanner, P. A. Advanced Red Phosphors for White Light-Emitting Diodes. *J. Mater. Chem. C* **2016**, *4*, 8611–8623.

(2) Qian, G.; Wang, Z. Y. Near-Infrared Organic Compounds and Emerging Applications. *Chem. - Asian J.* **2010**, *5*, 1006–1029.

(3) Guo, Z.; Park, S.; Yoon, J.; Shin, I. Recent Progress in the Development of Near-Infrared Fluorescent Probes for Bioimaging Applications. *Chem. Soc. Rev.* **2014**, *43*, 16–29.

(4) Xiang, H.; Cheng, J.; Ma, X.; Zhou, X.; Chruma, J. J. Near-Infrared Phosphorescence: Materials and Applications. *Chem. Soc. Rev.* **2013**, *42*, 6128–6185.

(5) Zhang, Y.; Luo, Q.; Zheng, W.; Wang, Z.; Lin, Y.; Zhang, E.; Lu, S.; Xiang, J.; Zhao, Y.; Wang, F. Luminescent Cyclometallated Platinum(II) Complexes: Highly Promising EGFR/DNA Probes and Dual-Targeting Anticancer Agents. *Inorg. Chem. Front.* **2018**, *5*, 413–424.

(6) Baggaley, E.; Weinstein, J. A.; Williams, J. A. G. Time-Resolved Emission Imaging Microscopy Using Phosphorescent Metal Complexes: Taking FLIM and PLIM to New Lengths. *Struc. Bond.* **2015**, *165*, 205–256.

(7) Chi, Y.; Chou, P.-T. Transition-Metal Phosphors with Cyclometalating Ligands: Fundamentals and Applications. *Chem. Soc. Rev.* **2010**, *39*, 638–655.

(8) Gray, T. G.; Rudzinski, C. M.; Nocera, D. G.; Holm, R. H. Highly Emissive Hexanuclear Rhenium(III) Clusters Containing the Cubic Cores $[Re_6S_8]^{2+}$ and $[Re_6Se_8]^{2+}$. *Inorg. Chem.* **1999**, *38*, 5932–5933.

(9) Molard, Y.; Dorson, F.; Brylev, K. A.; Shestopalov, M. A.; Le Gal, Y.; Cordier, S.; Mironov, Y. V.; Kitamura, N.; Perrin, C. Red-NIR Luminescent Hybrid Poly(Methyl Methacrylate) Containing Covalently Linked Octahedral Rhenium Metallic Clusters. *Chem. - Eur. J.* **2010**, *16*, 5613–5619.

(10) Tung, Y.-L.; Lee, S.-W.; Chi, Y.; Chen, L.-S.; Shu, C.-F.; Wu, F.-I.; Carty, A. J.; Chou, P.-T.; Peng, S.-M.; Lee, G.-H. Organic Light-Emitting Diodes Based on Charge-Neutral Ru^{II} Phosphorescent Emitters. *Adv. Mater.* **2005**, *17*, 1059–1064.

(11) Carlson, B.; Phelan, G. D.; Kaminsky, W.; Dalton, L.; Jiang, X.; Liu, S.; Jen, A. K. Y. Divalent Osmium Complexes: Synthesis, Characterization, Strong Red Phosphorescence, and Electrophosphorescence. *J. Am. Chem. Soc.* **2002**, *124*, 14162–14172.

(12) Lai, P.-N.; Teets, T. S. Ancillary Ligand Effects on Red-Emitting Cyclometalated Iridium Complexes. *Chem. - Eur. J.* **2019**, *25*, 6026–6037.

(13) Stonelake, T. M.; Phillips, K. A.; Otaif, H. Y.; Edwardson, Z. C.; Horton, P. N.; Coles, S. J.; Beames, J. M.; Pope, S. J. A. Spectroscopic and Theoretical Investigation of Color Tuning in Deep-Red Luminescent Iridium(III) Complexes. *Inorg. Chem.* **2020**, *59*, 2266–2277.

(14) Wu, W.; Guo, H.; Wu, W.; Ji, S.; Zhao, J. Long-Lived Room Temperature Deep-Red/Near-IR Emissive Intraligand Triplet Excited State (^{3}IL) of Naphthalimide in Cyclometalated Platinum(II) Complexes and Its Application in Upconversion. *Inorg. Chem.* **2011**, *50*, 11446–11460.

(15) Zhang, Y.; Meng, F.; You, C.; Yang, S.; Xiong, W.; Wang, Y.; Su, S.; Zhu, W. Achieving NIR Emission for Tetradentate Platinum(II) Salophen Complexes by Attaching Dual Donor-Accepter Frameworks in the Heads of Salophen. *Dyes Pigm.* **2017**, *138*, 100–106.

(16) Zhang, Y.; Yin, Z.; Meng, F.; Yu, J.; You, C.; Yang, S.; Tan, H.; Zhu, W.; Su, S. Tetradentate Pt(II) 3,6-Substituted Salophen Complexes: Synthesis and Tuning Emission from Deep-Red to near Infrared by Appending Donor-Acceptor Framework. *Org. Electron.* **2017**, *50*, 317–324.

(17) Xiong, W.; Meng, F.; You, C.; Wang, P.; Yu, J.; Wu, X.; Pei, Y.; Zhu, W.; Wang, Y.; Su, S. Molecular Isomeric Engineering of Naphthyl-Quinoline-Containing Dinuclear Platinum Complexes to Tune Emission from Deep Red to near Infrared. *J. Mater. Chem. C* **2019**, *7*, 630–638.

(18) Gernert, M.; Balles-Wolf, L.; Kerner, F.; Mueller, U.; Schmiedel, A.; Holzapfel, M.; Marian, C. M.; Pflaum, J.; Lambert, C.; Steffen, A. Cyclic (Amino)(Aryl)Carbenes Enter the Field of Chromophore Ligands: Expanded π System Leads to Unusually Deep Red Emitting CuI Compounds. *J. Am. Chem. Soc.* **2020**, *142*, 8897–8909.

(19) Li, L.-K.; Tang, M.-C.; Cheung, W.-L.; Lai, S.-L.; Ng, M.; Chan, C. K.-M.; Chan, M.-Y.; Yam, V. W.-W. Rational Design Strategy for the Realization of Red- to Near-Infrared-Emitting Alkynylgold(III) Complexes and Their Applications in Solution-Processable Organic Light-Emitting Devices. *Chem. Mater.* **2019**, *31*, 6706–6714.

(20) Li, K.; Tong, G. S. M.; Wan, Q.; Cheng, G.; Tong, W.-Y.; Ang, W.-H.; Kwong, W.-L.; Che, C.-M. Highly Phosphorescent Platinum(II) Emitters: Photophysics, Materials and Biological Applications. *Chem. Sci.* **2016**, *7*, 1653–1673.

(21) *Highly Efficient OLEDs with Phosphorescent Materials*; Yersin, H., Series Ed.; Wiley-VCH: Weinheim, Germany, **2007**.

(22) Cebrian, C.; Mauro, M. Recent Advances in Phosphorescent Platinum Complexes for Organic Light-Emitting Diodes. *Beilstein J. Org. Chem.* **2018**, *14*, 1459–1481.

(23) Kalinowski, J.; Fattori, V.; Cocchi, M.; Williams, J. A. G. Light-Emitting Devices Based on Organometallic Platinum Complexes as Emitters. *Coord. Chem. Rev.* **2011**, *255*, 2401–2425.

(24) Baggaley, E.; Weinstein, J. A.; Williams, J. A. G. Lighting the Way to See Inside the Live Cell With Luminescent Transition Metal Complexes. *Coord. Chem. Rev.* **2012**, *256*, 1762–1785.

(25) Mauro, M.; Aliprandi, A.; Septiadi, D.; Kehr, N. S.; De Cola, L. When Self-Assembly Meets Biology: Luminescent Platinum Complexes for Imaging Applications. *Chem. Soc. Rev.* **2014**, *43* (12), 4144–4166.

(26) Chen, Y.; Guan, R.; Zhang, C.; Huang, J.; Ji, L.; Chao, H. Two-Photon Luminescent Metal Complexes for Bioimaging and Cancer Phototherapy. *Coord. Chem. Rev.* **2016**, *310*, 16–40.

(27) Zhao, Q.; Li, F.; Huang, C. Phosphorescent Chemosensors Based on Heavy-Metal Complexes. *Chem. Soc. Rev.* **2010**, *39*, 3007–3030.

(28) Lai, S.-W.; Chan, M. C.-W.; Cheung, T.-C.; Peng, S.-M.; Che, C.-M. Probing d^8-d^8 Interactions in Luminescent Mono- and Binuclear Cyclometalated Platinum(II) Complexes of 6-Phenyl-2,2'-Bipyridines. *Inorg. Chem.* **1999**, *38*, 4046–4055.

(29) Cocchi, M.; Kalinowski, J.; Virgili, D.; Williams, J. A. G. Excimer-Based Red/Near-Infrared Organic Light-Emitting Diodes with Very High Quantum Efficiency. *Appl. Phys. Lett.* **2008**, *92*, 113302/1-113302/3.

(30) Baldo, M. A.; O'Brien, D. F.; You, Y.; Shoustikov, A.; Sibley, S.; Thompson, M. E.; Forrest, S. R. Highly Efficient Phosphorescent Emission from Organic Electroluminescent Devices. *Nature* **1998**, *395*, 151–154.

(31) Montes, V. A.; Pérez-Bolívar, C.; Agarwal, N.; Shinar, J.; Anzenbacher, P. Molecular-Wire Behavior of OLED Materials: Exciton Dynamics in Multichromophoric Alq_3-Oligofluorene-Pt(II)Porphyrin Triads. *J. Am. Chem. Soc.* **2006**, *128*, 12436–12438.

(32) Paul-Roth, C. O.; Drouet, S.; Merhi, A.; Williams, J. A. G.; Gildea, L. F.; Pearson, C.; Petty, M. C. Synthesis of Platinum Complexes of Fluorenyl-Substituted Porphyrins Used as Phosphorescent Dyes for Solution-Processed Organic Light-Emitting Devices. *Tetrahedron* **2013**, *69*, 9625–9632.

(33) Zhao, D.; Huang, C.-C.; Liu, X.-Y.; Song, B.; Ding, L.; Fung, M.-K.; Fan, J. Efficient OLEDs with Saturated Yellow and Red Emission Based on Rigid Tetradentate Pt(II) Complexes. *Org. Electron.* **2018**, *62*, 542–547.

(34) McKenzie, L. K.; Sazanovich, I. V.; Baggaley, E.; Bonneau, M.; Guerchais, V.; Williams, J. A. G.; Weinstein, J. A.; Bryant, H. E. Metal Complexes for Two-Photon Photodynamic Therapy: A Cyclometallated Iridium Complex Induces Two-Photon Photosensitization of Cancer Cells under Near-IR Light. *Chem. - Eur. J.* **2017**, *23*, 234–238.

(35) Colombo, A.; Fontani, M.; Dragonetti, C.; Roberto, D.; Williams, J. A. G.; Scotto di Perrotolo, R.; Casagrande, F.; Barozzi, S.; Polo, S. A Highly Luminescent Tetrahydrocurcumin Ir(III) Complex with Remarkable Photoactivated Anticancer Activity. *Chem. - Eur. J.* **2019**, *25*, 7948–7952.

(36) Liu, Y.; Meng, X.; Bu, W. Upconversion-Based Photodynamic Cancer Therapy. *Coord. Chem. Rev.* **2019**, *379*, 82–98.

(37) Wu, W.; Sun, J.; Ji, S.; Wu, W.; Zhao, J.; Guo, H. Tuning the Emissive Triplet Excited States of Platinum(II) Schiff Base Complexes with Pyrene, and Application for Luminescent Oxygen Sensing and Triplet-Triplet-Annihilation Based Upconversions. *Dalton Trans.* **2011**, *40*, 11550–11561.

(38) Mandapati, P.; Braun, J. D.; Killeen, C.; Davis, R. L.; Williams, J. A. G.; Herbert, D. E. Luminescent Platinum(II) Complexes of *N^N^N* Amido Ligands with Benzannulated *N*-Heterocyclic Donor Arms: Quinolines Offer Unexpectedly Deeper Red Phosphorescence than Phenanthridines. *Inorg. Chem.* **2019**, *58*, 14808–14817.

(39) Mondal, R.; Giesbrecht, P. K.; Herbert, D. E. Nickel(II), Copper(I) and Zinc(II) Complexes Supported by a (4-Diphenylphosphino)Phenanthridine Ligand. *Polyhedron* **2016**, *108*, 156–162.

(40) Lee, C.-I.; Zhou, J.; Ozerov, O. V. Catalytic Dehydrogenative Borylation of Terminal Alkynes by a SiNN Pincer Complex of Iridium. *J. Am. Chem. Soc.* **2013**, *135*, 3560–3566.

(41) We adopt the IUPAC numbering system for quinolines and phenanthridines, as illustrated in Scheme 1 for $\mathbf{L1}^{\mathbf{R,R}}$ and $\mathbf{L3}^{\mathbf{R,R}}$.

(42) Peters, J. C.; Harkins, S. B.; Brown, S. D.; Day, M. W. Pincer-like Amido Complexes of Platinum, Palladium, and Nickel. *Inorg. Chem.* **2001**, *40*, 5083–5091.

(43) Mandapati, P.; Giesbrecht, P. K.; Davis, R. L.; Herbert, D. E. Phenanthridine-Containing Pincer-like Amido Complexes of Nickel, Palladium, and Platinum. *Inorg. Chem.* **2017**, *56,* 3674–3685.

(44) Braun, J. D.; Lozada, I. B.; Kolodziej, C.; Burda, C.; Newman, K. M. E.; van Lierop, J.; Davis, R. L.; Herbert, D. E. Iron(II) Coordination Complexes with Panchromatic Absorption and Nanosecond Charge-Transfer Excited State Lifetimes. *Nat. Chem.* **2019**, *11*, 1144–1150.

(45) Hanson, K.; Roskop, L.; Djurovich, P. I.; Zahariev, F.; Gordon, M. S.; Thompson, M. E. A Paradigm for Blue- or Red-Shifted Absorption of Small Molecules Depending on the Site of π-Extension. *J. Am. Chem. Soc.* **2010**, *132*, 16247–16255.

(46) Liu, B.; Lystrom, L.; Brown, S. L.; Hobbie, E. K.; Kilina, S.; Sun, W. Impact of Benzannulation Site at the Diimine (*N^N*) Ligand on the Excited-State Properties and Reverse Saturable Absorption of Biscyclometalated Iridium(III) Complexes. *Inorg. Chem.* **2019**, *58*, 5483–5493.

(47) Mondal, R.; Lozada, I. B.; Davis, R. L.; Williams, J. A. G.; Herbert, D. E. Site-Selective Benzannulation of N-Heterocycles in Bidentate Ligands Leads to Blue-Shifted Emission from $[(P\text{^}N)\text{Cu}]_2(\mu\text{-X})_2$ Dimers. *Inorg. Chem.* **2018**, *57*, 4966–4978.

(48) Zander, M. The Significance of Donor-Acceptor Interactions in the External Heavy Atom Effect of Silver Nitrate on the Luminescence Behavior of Aza-Aromatic Systems and Carbazoles. *Z. Naturforsch. A* **1978**, *33*, 998–1000.

(49) Frey, J.; Curchod, B. F. E.; Scopelliti, R.; Tavernelli, I.; Rothlisberger, U.; Nazeeruddin, M. K.; Baranoff, E. Structure-Property Relationships Based on Hammett Constants in

Cyclometalated Iridium(III) Complexes: Their Application to the Design of a Fluorine-Free FIrPic-Like Emitter. *Dalton Trans.* **2014**, *43*, 5667–5679.

(50) Hansch, C.; Leo, A.; Taft, R. W. A Survey of Hammett Substituent Constants and Resonance and Field Parameters. *Chem. Rev.* **1991**, *91*, 165–195.

(51) Dedeian, K.; Djurovich, P. I.; Garces, F. O.; Carlson, G.; Watts, R. J. A New Synthetic Route to the Preparation of a Series of Strong Photoreducing Agents: Fac-Tris-Ortho-Metalated Complexes of Iridium(III) with Substituted 2-Phenylpyridines. *Inorg. Chem.* **1991**, *30*, 1685–1687.

(52) Brulatti, P.; Gildea, R. J.; Howard, J. A. K.; Fattori, V.; Cocchi, M.; Williams, J. A. G. Luminescent Iridium(III) Complexes with *N^C^N*-Coordinated Terdentate Ligands: Dual Tuning of the Emission Energy and Application to Organic Light-Emitting Devices. *Inorg. Chem.* **2012**, *51*, 3813–3826.

(53) Englman, R.; Jortner, J. Energy Gap Law for Radiationless Transitions in Large Molecules. *Mol. Phys.* **1970**, *18*, 145–164.

(54) Caspar, J. V.; Kober, E. M.; Sullivan, B. P.; Meyer, T. J. Application of the Energy Gap Law to the Decay of Charge-Transfer Excited States. *J. Am. Chem. Soc.* **1982**, *104*, 630–632.

(55) Caspar, J. V.; Meyer, T. J. Application of the Energy Gap Law to Nonradiative, Excited-State Decay. *J. Phys. Chem.* **1983**, *87*, 952–957.

(56) Whittle, C. E.; Weinstein, J. A.; George, M. W.; Schanze, K. S. Photophysics of Diimine Platinum(II) Bis-Acetylide Complexes. *Inorg. Chem.* **2001**, *40*, 4053–4062.

(57) Ibrahim-Ouali, M.; Dumur, F. Recent Advances on Metal-Based Near-Infrared and Infrared Emitting OLEDs. *Molecules* **2019**, *24*, 1412.

(58) Borisov, S. M.; Nuss, G.; Haas, W.; Saf, R.; Schmuck, M.; Klimant, I. New NIR-Emitting Complexes of Platinum(II) and Palladium(II) With Fluorinated Benzoporphyrins. *J. Photochem. Photobiol. A* **2009**, *201*, 128–135.

(59) Tuong Ly, K.; Chen-Cheng, R.-W.; Lin, H.-W.; Shiau, Y.-J.; Liu, S.-H.; Chou, P.-T.; Tsao, C.-S.; Huang, Y.-C.; Chi, Y. Near-Infrared Organic Light-Emitting Diodes With Very High External Quantum Efficiency and Radiance. *Nat. Photon.* **2017**, *11*, 63–68.

(60) Kabir, E.; Wu, Y.; Sittel, S.; Nguyen, B.-L.; Teets, T. S. Improved Deep-Red Phosphorescence in Cyclometalated Iridium Complexes via Ancillary Ligand Modification. *Inorg. Chem. Front.* **2020**, *7*, 1362–1373.

(61) Medina Padilla, M.; Castro Morera, A.; Sanchez-Quesada, J.; Garcia Palomero, E.; Alonso Cascon, M.; Herrero Santos, S.; Vela Ruiz, M.; Usan Egea, P.; Rodriguez Villanueva, A.

L. Triple Substituted Phenanthroline Derivatives for the Treatment of Neurodegenerative or Haematological Diseases or Conditions, or Cancer. US20110306631A1, **2011**.

(62) Mandapati, P.; Braun, J. D.; Sidhu, B. K.; Wilson, G.; Herbert, D. E. Catalytic C–H Bond Alkylation of Azoles with Alkyl Halides Mediated by Nickel(II) Complexes of Phenanthridine-Based *N^N¯^N* Pincer Ligands. *Organometallics* **2020**, *39*, 1989–1997.

(63) Clark, H. C.; Manzer, L. E. Reactions of (π-1,5-Cyclooctadiene)Organoplatinum(II) Compounds and the Synthesis of Perfluoroalkylplatinum Complexes. *J. Organomet. Chem.* **1973**, *59*, 411–428.

(64) Bruker-AXS. *APEX3 V2016.1-0*; Madison, Wisconsin, USA, 2016.

(65) Sheldrick, G. M. A Short History of SHELX. *Acta Cryst.* **2008**, *A64*, 112–122.

(66) Spek, A. L. Structure Validation in Chemical Crystallography. *Acta Cryst.* **2009**, *D65*, 148–155.

(67) Frisch, M. J.; Trucks, G. W.; Schlegel, H. B.; Scuseria, G. E.; Robb, M. A.; Cheeseman, J. R.; Scalmani, G.; Barone, V.; Petersson, G. A.; Nakatsuji, H.; Li, X.; Caricato, M.; Marenich, A. V.; Bloino, J.; Janesko, B. G.; Gomperts, R.; Mennucci, B.; Hratchian, H. P.; Ortiz, J. V.; Izmaylov, A. F.; Sonnenberg, J. L.; Williams; Ding, F.; Lipparini, F.; Egidi, F.; Goings, J.; Peng, B.; Petrone, A.; Henderson, T.; Ranasinghe, D.; Zakrzewski, V. G.; Gao, J.; Rega, N.; Zheng, G.; Liang, W.; Hada, M.; Ehara, M.; Toyota, K.; Fukuda, R.; Hasegawa, J.; Ishida, M.; Nakajima, T.; Honda, Y.; Kitao, O.; Nakai, H.; Vreven, T.; Throssell, K.; Montgomery Jr., J. A.; Peralta, J. E.; Ogliaro, F.; Bearpark, M. J.; Heyd, J. J.; Brothers, E. N.; Kudin, K. N.; Staroverov, V. N.; Keith, T. A.; Kobayashi, R.; Normand, J.; Raghavachari, K.; Rendell, A. P.; Burant, J. C.; Iyengar, S. S.; Tomasi, J.; Cossi, M.; Millam, J. M.; Klene, M.; Adamo, C.; Cammi, R.; Ochterski, J. W.; Martin, R. L.; Morokuma, K.; Farkas, O.; Foresman, J. B.; Fox, D. J. *Gaussian 16 Rev. C.01*; Wallingford, CT, **2016**.

(68) Zhao, Y.; Truhlar, D. G. The M06 Suite of Density Functionals for Main Group Thermochemistry, Thermochemical Kinetics, Noncovalent Interactions, Excited States, and Transition Elements: Two New Functionals and Systematic Testing of Four M06-Class Functionals and 12 Other Functionals. *Theor. Chem. Acc.* **2008**, *120*, 215–241.

(69) Dunning, T. H.; Hay, P. J. In *Modern Theoretical Chemistry*; Schaefer III, H. F., Ed.; Plenum, New York, **1977**; Vol. 3, pp 1–28.

(70) Tomasi, J.; Mennucci, B.; Cammi, R. Quantum Mechanical Continuum Solvation Models. *Chem. Rev.* **2005**, *105*, 2999–3094.

(71) Hirshfeld, F. L. Bonded-Atom Fragments for Describing Molecular Charge Densities. *Theor. Chim. Acta* **1977**, *44*, 129–138.

(72) Lu, T.; Chen, F. Multiwfn: A Multifunctional Wavefunction Analyzer. *J. Comput. Chem.* **2012**, *33*, 580–592.

(73) Hanwell, M. D.; Curtis, D. E.; Lonie, D. C.; Vandermeersch, T.; Zurek, E.; Hutchison, G. R. Avogadro: An Advanced Semantic Chemical Editor, Visualization, and Analysis Platform. *J. Cheminf.* **2012**, *4*, 17.

(74) O'Boyle, N. M.; Tenderholt, A. L.; Langner, K. M. Software News and Updates Cclib: A Library for Package-Independent Computational Chemistry Algorithms. *J. Comput. Chem.* **2008**, *29*, 839–845.

(75) Allouche, A.-R. Gabedit - A Graphical User Interface for Computational Chemistry Softwares. *J. Comput. Chem.* **2011**, *32*, 174–182.

For Table of Contents Only

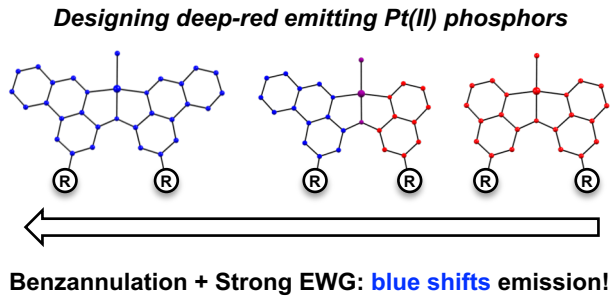

TOC Synopsis

A series of deep-red emitting Pt(II) phosphors is presented. These charge-neutral complexes have the general structure (*N*^*N*⁻^*N*)PtCl and are supported by benzannulated diarylamido ligand scaffolds bearing substituted quinolinyl and/or phenanthridinyl arms. In contradiction to conventional assumptions, benzannulation counter-intuitively but markedly blue-shifts emission from the metal complexes with identical substitution patterns. This effect can be further tuned by incorporation of electron-releasing or electron-withdrawing substituents in either the phenanthridine 2-position or quinoline 6-position.